Journal of Marine Research, 55, 223–275, 1997

Large-scale circulation with small diapycnal diffusion: The two-thermocline limit

by R. M. Samelson[1] and Geoffrey K. Vallis[2]

ABSTRACT

The structure and dynamics of the large-scale circulation of a single-hemisphere, closed-basin ocean with small diapycnal diffusion are studied by numerical and analytical methods. The investigation is motivated in part by recent differing theoretical descriptions of the dynamics that control the stratification of the upper ocean, and in part by recent observational evidence that diapycnal diffusivities due to small-scale turbulence in the ocean thermocline are small (~ 0.1 cm^2 s^{-1}). Numerical solutions of a computationally efficient, three-dimensional, planetary geostrophic ocean circulation model are obtained in a square basin on a mid-latitude β-plane. The forcing consists of a zonal wind stress (imposed meridional Ekman flow) and a surface heat flux proportional to the difference between surface temperature and an imposed air temperature. For small diapycnal diffusivities (vertical: $\kappa_v \sim 0.1 - 0.5$ cm^2 s^{-1}, horizontal: $\kappa_h \sim 10^5 - 5 \times 10^6$ cm^2 s^{-1}), two distinct thermocline regimes occur. On isopycnals that outcrop in the subtropical gyre, in the region of Ekman downwelling, a ventilated thermocline forms. In this regime, advection dominates diapycnal diffusion, and the heat balance is closed by surface cooling and convection in the northwest part of the subtropical gyre. An 'advective' vertical scale describes the depth to which the wind-driven motion penetrates, that is, the thickness of the ventilated thermocline. At the base of the wind-driven fluid layer, a second thermocline forms beneath a layer of vertically homogeneous fluid ('mode water'). This 'internal' thermocline is intrinsically diffusive. An 'internal boundary layer' vertical scale (proportional to $\kappa_v^{1/2}$) describes the thickness of this internal thermocline. Two varieties of subtropical mode waters are distinguished. The temperature difference across the ventilated thermocline is determined to first order by the meridional air temperature difference across the subtropical gyre. The temperature difference across the internal thermocline is determined to first order by the temperature difference across the subpolar gyre. The diffusively-driven meridional overturning cell is effectively confined below the ventilated thermocline, and driven to first order by the temperature difference across the internal thermocline, not the basin-wide meridional air temperature difference. Consequently, for small diapycnal diffusion, the abyssal circulation depends to first order only on the wind-forcing and the subpolar gyre air temperatures. The numerical solutions have a qualitative resemblance to the observed structure of the North Atlantic in and above the main thermocline (that is, to a depth of roughly 1500 m). Below the main thermocline, the predicted stratification is much weaker than observed.

1. Woods Hole Oceanographic Institution, Woods Hole, Massachusetts, 02543, U.S.A.
2. University of California, Santa Cruz, California, 95064, U.S.A.

1. Introduction

A fundamental goal of physical oceanography is to describe and understand the large-scale circulation and stratification of the ocean, that is, the features with horizontal scale comparable to that of the oceans themselves. In its simplest general form, the associated theoretical problem is to determine the steady, planetary-scale response of a thin, rapidly-rotating layer of fluid to wind and buoyancy forcing at its upper surface, and to relate the components of the response to large-scale oceanographic observations. An important step toward the solution of this 'thermocline problem' was the derivation by scale asymptotics of a simplified set of equations for the planetary-scale motion, the planetary-geostrophic or 'thermocline' equations (Robinson and Stommel, 1959; Welander, 1959; Phillips, 1963). Most theoretical progress on the thermocline problem has followed from the analysis of various forms of these equations.

Two distinct classes of theories for the subtropical thermocline have emerged from this approach. These may be termed the 'ventilated thermocline' and 'internal boundary layer' theories. The ventilated thermocline theory is founded on the ideal fluid thermocline equations, proposed by Welander (1959) as an advective (adiabatic) model of the interior dynamics. This model was given renewed impetus by the demonstration by Luyten *et al.* (1983) that solutions of the ideal equations can be found that satisfy independent surface boundary conditions on density and vertical velocity and have vanishing motion at depth, a combination that had previously proved elusive (Welander, 1971a). In this picture, the surface density is given as an upper boundary condition in the subtropical gyre, and the surface fluid is advected downward into the ocean interior by Ekman downwelling. The Sverdrup transport balance and conservation of potential vorticity by the adiabatic interior flow then determines, with some additional assumptions, the three-dimensional structure of the upper ocean (Luyten *et al.,* 1983; Huang, 1988; 1991). The internal boundary layer (or 'frontal thermocline') theory is founded on the diffusive thermocline equations proposed by Robinson and Stommel (1959). These differ from the ideal fluid thermocline equations by the addition of a vertical thermal diffusion that is presumed to represent the first-order effect of small-scale motions on the large-scale flow. In this picture, the subtropical thermocline is an internal boundary layer or front that forms at the vertical convergence of two different homogeneous water types, warm surface fluid above and cold abyssal fluid below. Stommel and Webster (1962) used these ideas to develop a quantitative theoretical model for the diffusively-driven thermohaline circulation. This theory has recently been revived and extended by Salmon (1990) and Young and Ierley (1986).

These two theories appear to give conflicting descriptions of the structure and dynamics of the subtropical ocean thermocline. The ventilated thermocline theory, which (in its essential form) has zero diapycnal diffusion, produces a complex three-dimensional density field. The internal boundary layer theory, which is intrinsically diffusive, predicts instead the development of an arbitrarily thin, frontal thermocline in the limit of small diapycnal diffusion. The dichotomy between the two theories has been noted by Salmon (1990) and Salmon and Hollerbach (1991), and further explored by Hood and Williams

(1996), while the fundamental difference between the underlying dynamics of Welander (1959) and Robinson and Stommel (1959) has long been evident (Veronis, 1969). A third, related theory, for large-scale motion in the deep 'unventilated' thermocline, predicts that the stratification of recirculating fluid will be modified by eddy fluxes that tend to homogenize the potential vorticity (Rhines and Young, 1982). The modified stratification predicted by this theory depends on the imposed 'background' stratification beneath the wind-driven fluid, which is presumed to be controlled by other processes. Since these processes are not explicitly represented in the Rhines-Young theory, the small eddy-flux limit of the Rhines-Young theory is in essence a singular perturbation not of the ventilated or internal boundary layer thermocline theories, but of an arbitrary background state that possesses closed geostrophic contours; the fixed background stratification allows exposition of the theory with quasi-geostrophic equations. In contrast, the adiabatic planetary geostrophic equations of the ventilated thermocline theory may be viewed as a singular perturbation of the fundamental equations of the internal boundary layer theory, in which the former are obtained from the latter by setting the vertical diffusivity to zero. For this reason, the Rhines-Young description does not lead to an analogous direct dichotomy with either of the two aforementioned thermocline theories, although it points to a more general conflict between theories that do and do not include certain representations of eddy fluxes. In the present study, we purposely attempt to obtain results in which the effects of time-dependent mesoscale motions are essentially absent, in order to focus on the interaction of the large-scale flow and small-scale turbulent diapycnal diffusion.

If diapycnal diffusion in the ocean were sufficiently large, neither the adiabatic ventilated theory nor the small-diffusion limit of the internal boundary layer theory would be directly relevant to the ocean thermocline, and the resolution of the conflict between them would be of little practical interest. However, recent microstructure and tracer dispersion measurements (Gregg, 1987; Ledwell *et al.*, 1993; Toole *et al.*, 1994) suggest that vertical (diapycnal) diffusivities in the ocean interior are sufficiently small (~ 0.1 cm^2 s^{-1}) that the two theories predict substantially different vertical scales for the thermocline (see Section 4). Moreover, these diffusivity estimates are an order of magnitude smaller than values typically used in numerical models of the large-scale ocean circulation. Since neither thermocline theory describes closed circulations that satisfy a complete set of boundary conditions in an entire basin, and because of the large diffusivities typically used in the numerical models, the relation between the theories and the closed-basin circulation has generally remained uncertain, despite some important specific comparisons (e.g., Cox and Bryan, 1984; Cox, 1985). Consequently, there are good reasons to examine the large-scale closed-basin circulation that arises for small diapycnal diffusion.

A primary goal of the present study is therefore to explore and reconcile the two differing thermocline theories, using a simple model of large-scale circulation in a closed basin. The model is based on the planetary geostrophic formulation proposed by Samelson and Vallis (1997). The model equations support a frictional western boundary layer that is adiabatic to

first order, and allow efficient and well-posed numerical integration in a closed domain with a physically appropriate set of boundary conditions. We are interested here in the thermocline structure that arises in the model when friction and horizontal diffusion are sufficiently small that the interior flow may be described locally by solutions of the thermocline equations. The present contribution is a continuation of the studies of wind and buoyancy-forced closed-basin planetary geostrophic ocean circulation models begun by Colin de Verdiere (1988, 1989) and Salmon (1990). Zhang *et al.* (1992) and Winton and Sarachik (1993) have recently studied related planetary geostrophic closed-basin models, with a greater emphasis on saline effects.

We find that for small diapycnal diffusivities (vertical: $\kappa_v \sim 0.1 - 0.5$ cm^2 s^{-1}, horizontal: $\kappa_h \sim 10^5 - 5 \times 10^6$ cm^2 s^{-1}), two distinct thermocline regimes occur in the subtropical gyre, as an internal boundary layer thermocline forms at the base of the ventilated thermocline (Fig. 1). This result is consistent with the idea, proposed on the basis of scale analysis by Welander (1971b), that diffusion becomes dynamically important at some depth beneath an approximately adiabatic near-surface flow. It has been partly anticipated by the heuristic arguments of Pedlosky (1979, p. 422), the analysis of flow regimes in a planetary geostrophic model by Colin de Verdiere (1989), and the discussion of similarity solutions by Salmon and Hollerbach (1991). We find also that the internal thermocline is a recirculation regime (so the explicit western boundary layer plays an important role), and that potential vorticity on isopycnals in the internal thermocline is approximately uniform. However, the potential vorticity in the recirculation regime is primarily controlled by vertical diffusion, not horizontal diffusion (which has been purposely minimized in the present calculations) as in the homogenization theory. A shallow thermostad ('mode water') forms at the base of the ventilated thermocline.

The model formulation is presented in Section 2. The general structure of the small-diffusion solutions is described in Section 3 and interpreted using scaling arguments in Section 4. The dependence of the circulation on meridional air temperature is discussed in Section 5. Sections 6 and 7 contain explicit comparisons with the internal boundary layer and ventilated thermocline theories, respectively. A brief discussion of the western boundary current is included in Section 8. The solutions are compared with observations in Section 9, and the results are summarized in Section 10.

2. Model formulation

The model consists of an interior domain with nearly-geostrophic flow capped by a surface boundary layer of fixed depth containing the frictionally-driven Ekman flow. The model equations are supplemented by a convective adjustment scheme. The interior and surface boundary layer models are described below. The numerical implementation is summarized in an appendix.

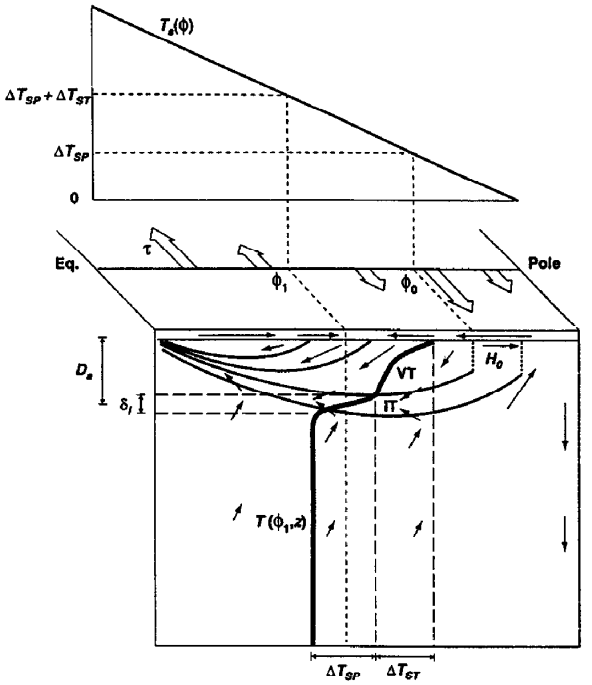

Figure 1. A schematic picture of the large-scale circulation and the thermocline regimes in a simply-connected, single-hemisphere ocean driven by wind-stress and differential heating, with small diapycnal diffusion. The upper part of the figure indicates the zonal wind-forcing τ (broad arrows) and the atmospheric temperature profile $T_s(\phi)$, where ϕ is latitude. The idealized meridional section below is at a mid-basin longitude. The latitude ϕ_0 is the latitude of zero Ekman pumping at the subtropical-subpolar gyre boundary. The curve $T(\phi_1, z)$ (thick line) is a temperature profile at the latitude ϕ_1 (where it crosses the internal thermocline) in the central subtropical gyre. The arrows indicate the mid-basin circulation in the plane of the section. The thickness of the surface Ekman layer is exaggerated. The ventilated thermocline (VT) is an advective regime. Its thickness is the advective scale D_a, and the temperature difference across it is equal to $\Delta T_{ST} = T_s(\phi_1) - T_s(\phi_0)$. The internal thermocline (IT) is a diffusive regime at the base of the ventilated thermocline. Its thickness is the internal boundary layer scale δ_i, and the temperature difference across it is equal to $\Delta T_{SP} = T_s(\phi_0) - T_s(\text{Pole})$. H_0 is the depth of the mixed layer at the latitude ϕ_0. (Cf. Fig. 1 of Welander, 1971b.)

a. Interior equations. The interior equations are the hydrostatic-biharmonic diffusive planetary geostrophic equations proposed by Samelson and Vallis (1997), which are

$$-fv + p_x = -\epsilon u \tag{2.1}$$

$$-fu + p_y = -\epsilon v \tag{2.2}$$

$$p_z - T = 0 \tag{2.3}$$

$$u_x + v_y + w_z = 0 \tag{2.4}$$

$$T_t + uT_x + vT_y + wT_z = \kappa_v T_{zz} + \kappa_h \Delta_h T - \lambda \Delta_h^2 T \tag{2.5}$$

where

$$\Delta_h = \frac{\partial^2}{\partial x^2} + \frac{\partial^2}{\partial y^2}. \tag{2.6}$$

Here (u, v, w) are the (x, y, z)-components of velocity, t is time, p is pressure divided by a constant reference density ρ_0, T is temperature (with density $\rho = -T$, so that isothermal surfaces are also isopycnal surfaces, and thermal diffusion is always diapycnal; we often use the density terminology in dynamical contexts below), and subscripts x, y, z, and t denote partial derivatives. These equations satisfy boundary conditions on normal flow and normal heat flux at each rigid boundary (Samelson and Vallis, 1997). They form a computationally efficient alternative to the planetary geostrophic equations of Colin de Verdiere (1988, 1989) and Salmon (1990), both of which admit more general body forces and do not require biharmonic diffusion in the thermodynamic equation. The Coriolis parameter f is a linear function of y,

$$f = f_0 + \beta(y - y_0) \tag{2.7}$$

where β, f_0, and y_0 are constants. For the calculations described below, the diffusivities κ_v, κ_h, λ are positive constants, while the frictional parameter ϵ may be a function of x and y. Cartesian coordinates are used for simplicity, and the effects of salinity are neglected. The basin is square, with vertical lateral boundaries at $x = \{0, 1\}$ and $y = \{0, 1\}$, and a flat bottom at $z = 0$. The upper boundary of the interior domain at $z = 1$ is the base of the surface boundary layer. For numerical solution, these equations are supplemented by a convective adjustment scheme which removes static instabilities at each time step by vertically mixing grid-point fluid volumes to restore neutral stability.

The ideal fluid thermocline equations (Welander, 1959) may be obtained from (2.1)–(2.5) by setting $\epsilon = \kappa_v = \kappa_h = \lambda = 0$. The vertical diffusion term $\kappa_v T_{zz}$ in (2.5) is a traditional representation of the effect of turbulent mixing on the large-scale flow (Robinson and Stommel, 1959). The additional diabatic and frictional terms in (2.1)–(2.5) support the lateral boundary layers that allow solution of the equations in a closed basin, and damp unphysical interior instabilities (Samelson and Vallis, 1997). These terms are kept small in the solutions presented here in order to minimize their effect on the interior flow. Thus, the horizontal diffusivity κ_h is generally one or two orders of magnitude smaller than often-used values for lateral tracer diffusivities. Numerical parameter values are reported below.

The frictional-geostrophic relations (2.1) and (2.2) may be inverted for the horizontal velocities, giving

$$u = -\gamma(\epsilon p_x + f p_y), \qquad v = \gamma(f p_x - \epsilon p_y) \tag{2.8}$$

where $\gamma = (f^2 + \epsilon^2)^{-1}$. Thus, the linear horizontal drag drives ageostrophic flow down the pressure gradient. The angle that the flow makes with the lines of constant pressure on horizontal surfaces is fixed by the local values of ϵ and f, while the speed of the flow is locally proportional to the magnitude of the pressure gradient. A useful relation may be obtained by substituting these expressions into the continuity equation (2.4), which gives

$$\mathscr{H}(p) = w_z \tag{2.9}$$

where

$$\mathscr{H}(p) = \epsilon\gamma\Delta_h p + (f^2 - \epsilon^2)\gamma^2\beta p_x - 2\epsilon f\gamma^2\beta p_y \tag{2.10}$$

in the case of constant ϵ. The equation (2.9) is a form of the vorticity equation

$$\beta v - f w_z + (\epsilon v)_x - (\epsilon u)_y = 0. \tag{2.11}$$

The evolution equation for the potential vorticity $Q = f T_z$ is

$$\begin{aligned} Q_t + uQ_x + vQ_y + wQ_z = \kappa_v Q_{zz} + \kappa_h f\Delta_h(Q/f) - \lambda f\Delta_h^2(Q/f) \\ + \epsilon\gamma f(T_x^2 + T_y^2) - [(\epsilon v)_x - (\epsilon u)_y]Q/f, \end{aligned} \tag{2.12}$$

so potential vorticity is a Lagrangian invariant in the absence of friction and diffusion.

The no-flux condition on heat diffusion at lateral boundaries is a boundary condition on temperature,

$$-\kappa_h T_n + \lambda\Delta_h T_n = 0. \tag{2.13}$$

The vertical derivative of (2.8) yields the frictional-geostrophic analog of the thermal wind relation,

$$u_z = -\gamma(\epsilon T_x + f T_y), \qquad v_z = \gamma(f T_x - \epsilon T_y) \tag{2.14}$$

and, consequently, the no-normal-flow boundary condition implies a second boundary condition on temperature,

$$\epsilon T_n + f T_s = 0. \tag{2.15}$$

As argued elsewhere (Samelson and Vallis, 1997), it is the need to satisfy this second boundary condition on T (which is solved as a differential equation around the boundary) that motivates the introduction of the biharmonic diffusion term in (2.5). Requiring that horizontal diapycnal fluxes across the sloping isotherms of the western boundary current be minimized suggests the choice

$$\lambda = \lambda_0 = (\epsilon/\beta)^2\kappa_h, \tag{2.16}$$

and the solutions discussed below use this value of λ unless otherwise noted.

The generalization to $\epsilon > 0$ of Welander's (1971b) argument shows that the system (2.1)–(2.5) may be written as a single equation in the dependent variable M,

$$M_{zzt} - \gamma(fM_{zy} + \epsilon M_{zx})M_{zzx} + \gamma(fM_{zx} - \epsilon M_{zy})M_{zzy} + \mathscr{H}(M)M_{zzz} = \kappa_v M_{zzzz} + \kappa_h \Delta_h M_{zz} - \lambda \Delta_h^2 M_{zz} \tag{2.17}$$

where

$$M_z = p, \tag{2.18}$$

and the additional boundary conditions $M(z = 0) = 0$ and $w(z = 0) = 0$ have been imposed (Samelson and Vallis, 1997).

b. Surface boundary layer and air-sea fluxes. The upper boundary condition on temperature for the interior equations is obtained from a simple 'slab' model of a frictional surface boundary layer. The boundary layer is taken to have fixed depth δ_E, so the sea surface is at $z = 1 + \delta_E$. The surface boundary layer temperature T_E is obtained from a vertically integrated thermodynamic equation,

$$T_{Et} + (u_A T_E)_x + (v_A T_E)_y = (F_T - F_i)/\delta_E \tag{2.19}$$

where F_T is the air-sea flux and F_i is the flux through the base of the boundary layer. In order to allow the northward advection of warm surface boundary layer water by the western boundary current, the interior velocities at the base of the boundary layer are added to an Ekman flow to obtain the advective velocities (u_A, v_A) in (2.19),

$$(u_A, v_A) = (u_E, v_E) + (u, v)_{(z=1)}. \tag{2.20}$$

The Ekman flow (u_E, v_E) is specified to be meridional ($u_E = 0$) and of the form

$$v_E = (w_{E0}/2\pi\delta_E) \sin 2\pi y, \tag{2.21}$$

(where $0 \leq y \leq 1$), so the Ekman pumping is

$$w_E = \delta_E v_{Ey} = w_{E0} \cos 2\pi y. \tag{2.22}$$

Thus, the subtropical downwelling and subpolar upwelling regions cover the central half ($0.25 < y < 0.75$) and the northern quarter ($0.75 < y < 1$) of the domain, respectively. The southern, 'tropical' upwelling region ($0 < y < 0.25$) is required in order to bring the meridional Ekman flux to zero at the southern boundary. A more conventional (and probably more realistic) representation of the meridional distribution of interior Ekman upwelling might confine the tropical upwelling to a smaller region adjacent to the equator. We have chosen the present distribution in order to avoid imposing any horizontal boundary layer structure on the interior, and because the southern boundary of the domain lies north of the equator, so that the equatorial dynamics would not be appropriately represented in any case.

Including the advection by the interior flow in (2.20) is essentially equivalent to extending the interior horizontal momentum balance (2.1)–(2.2) for the pressure-driven flow through the surface boundary layer, while neglecting the vertical variation of the pressure in the boundary layer. This decomposition of the surface boundary layer velocity into a wind-driven Ekman component and a pressure-driven frictional-geostrophic component is consistent with the assumed linearity of the horizontal momentum equations, and the neglect of the vertical shear of the latter component is consistent with the condition $\delta_E \ll 1$. A vertical integral of (2.9) over the entire domain, including the surface boundary layer where (2.8) are supplemented by the Ekman flow component, then yields a diagnostic equation

$$\mathscr{H}(P) = w_E - W_0 \tag{2.23}$$

for the vertically integrated (barotropic) pressure, P, where

$$P = \int_0^1 p\, dz + \delta_E p(z = 1). \tag{2.24}$$

In (2.23), w_E is the Ekman pumping velocity from (2.22), and $W_0 = w(z = 0) = 0$ at the flat bottom boundary. Thus, P depends only on the imposed mechanical forcing, w_E.

The air-sea heat flux F_T is obtained from T_E and an imposed atmospheric surface temperature T_s using the simplified flux law (Haney, 1971)

$$F_T = -\gamma_{Ts}(T_E - T_s). \tag{2.25}$$

For the solutions discussed below, T_s is taken to be a piecewise-continuous linear function of y. The heat flux F_i through the base of the boundary layer is composed of an advective component and a parameterized diffusive component,

$$F_i = -w(z = 1)T_1 + \gamma_0(\kappa_v/\delta_E)[T_E - T(z = 1)], \tag{2.26}$$

and this serves as the upper boundary condition for the interior thermodynamic equation (2.5), which is solved in flux form. A temperature discontinuity is allowed at the base of the surface boundary layer, so that in (2.26), $T_1 = T(z = 1)$ if $w(z = 1) > 0$ and $T_1 = T_E$ from the frictional-geostrophic convergence in the surface layer. With κ_v and δ_E given, the nondimensional constant γ_0 determines the rate of diffusive heat transport from the surface layer into the interior.

The Ekman flow, rather than the wind stress, is specified in order to simplify the problem and because the equations (2.1)–(2.5) do not admit arbitrary forcing terms (Salmon, 1986; Samelson and Vallis, 1997). However, if the vertically integrated Ekman balance

$$(u_E, v_E) = (\tau^y, -\tau^x)/f\delta_E \tag{2.27}$$

is assumed to hold, where $\tau = (\tau^x, \tau^y)$ is the wind stress at the sea surface, then this balance may be inverted for the wind stress τ. For the solutions discussed below, the wind stress

obtained in this manner is zonal ($\tau^y = 0$), and has the form

$$\tau^x = \tau_0(f(y)/f_0) \sin 2\pi y, \qquad \tau_0 = -f_0 w_{E0}/2\pi. \tag{2.28}$$

Alternatively, a linear frictional drag as in (2.1)–(2.2) may also be taken to modify the Ekman balance, in which case the inferred wind stress pattern would include a small meridional component.

Some of the calculations reported below were initially carried out with a different surface boundary layer scheme, in which the vertical velocity at the base of the surface boundary layer was taken to be w_E, and the barotropic pressure in (2.24) was computed as the integral from $z = 0$ to $z = 1$, without the contribution from the surface boundary layer. Since the interior advection was retained in (2.20), this led to errors in the heat balance. Although the qualitative results were essentially unaffected, the effect on the temperature of the abyssal fluid was sufficiently large to warrant repeating most of the calculations with the present treatment. When results reported below are based on the previous boundary layer treatment, this is indicated.

c. Nondimensionalization. Appropriate dimensional values for the variables and parameters described above may be obtained using the following scales for depth, length, Coriolis parameter, density, gravity, and vertical velocity, respectively: $D = 5 \times 10^5$ cm, $L = 5 \times 10^8$ cm, $f_* = f(35\text{N}) = 8.4 \times 10^{-5}$ s^{-1}, $\rho_0 = 1$ g cm^{-3}, $g = 980$ cm s^{-2}, $W = 10^{-4}$ cm s^{-1}.

From these, the following dimensional scales may be derived for horizontal velocity, time, density variations, temperature variations, buoyancy frequency, heat flux and heat transport, respectively: $U = WL/D = 0.1$ cm s^{-1}, $t_* = D/W = L/U = 5 \times 10^9$ s $= 160$ yr, $\rho_* = (\rho_0 f_* UL)/(gD) = 8.6 \times 10^{-6}$ g cm^{-3} $\sim 0.01\ \sigma_\theta$, $T_* = \rho_*/(\rho_0 \alpha_T) = 0.086$ K, $N_0 = (g\rho_*/(\rho_0 D))^{1/2} = 1.3 \times 10^{-4}$ s^{-1} $= 0.075$ cph, $H_f = \rho_0 c_p WT_* = 0.34$ W m^{-2}, $H_F = H_f L^2 = 0.9 \times 10^{13}$ *W*, where the values $\alpha_T = 10^{-4}$ K^{-1} and $c_p = 4000\ J\ \text{kg}^{-1}\ K^{-1}$ have been used for the thermal expansibility and specific heat of sea water.

Dimensional scales for the vertical, horizontal, and biharmonic horizontal thermal diffusivities are then $K_v = WD = 50$ cm^2 s^{-1}, $K_h = UL = 5 \times 10^7$ cm^2 s^{-1}, $\Lambda = UL^3 = 1.25 \times 10^{25}$ cm^4 s^{-1}. The friction parameter ϵ and the air-sea flux coefficient γ_{Ts} are nondimensionalized by f and *W*, respectively. The nondimensional parameter $\gamma_0 = 2$ in all cases.

In the discussion below, nondimensional values of the parameters will generally be quoted, with corresponding dimensional values given parenthetically. Thus, $\kappa_v = 0.01$ (0.5 cm^2 s^{-1}) corresponds to nondimensional and dimensional vertical temperature diffusivities of 0.01 and 0.01×50 cm^2 s^{-1} $= 0.5$ cm^2 s^{-1}, respectively. The figures use nondimensional variables.

d. Method of solution. The equations may be solved as follows. The elliptic equation (2.23) may be solved for P by standard methods (e.g. relaxation techniques), subject to the

vertically-integrated no-normal-flow condition

$$\epsilon P_n + f P_s = 0 \tag{2.29}$$

(where the subscripts n and s denote the outward normal and right-handed tangential derivatives, respectively) at the lateral boundaries. For all the numerical solutions discussed below, the imposed Ekman pumping w_E is independent of time, so the elliptic equation (2.23) need be solved only once, at the beginning of the time-stepping integration. If the temperature T is known at a given time, the baroclinic pressure $p' \equiv p - P$ may be obtained by integrating the hydrostatic relation (2.3), and the velocities may be calculated from the pressure $p = p' + P$ using (2.8) and (2.4). With the boundary conditions (2.13) and (2.15), and with the velocities known, the thermodynamic equations (2.5) and (2.19) may be time-stepped to obtain the new temperature field. Static instabilities are removed after each time-step by the convective adjustment scheme. This process is then repeated indefinitely. The steady solutions discussed below were obtained by time-stepping the equations in this manner to effective equilibrium. Winton and Sarachik (1993) present numerical solutions of a similar hydrostatic planetary geostrophic thermohaline circulation model with linear horizontal drag and with $\kappa_h = \lambda = 0$ identically. The latter condition led to difficulties with the present solutions (Samelson and Vallis, 1997). Their numerical implementation required also that the tangential velocity at the boundary be obtained from an additional integral condition.

We take $f_0 = 1$, $\beta = \beta * L/f_* = 1.1$, corresponding to a northern hemisphere basin with a central latitude of 35N at $y = y_0 = 0.5$. Solutions are typically obtained at horizontal resolution of 64×64 grid points, giving a resolution of about 80 km for the square basin of side 5,000 km. In the vertical, we normally use 32 and sometimes 64 grid points, stretched in the vertical to give enhanced resolution in the thermocline. Note that the western boundary layer is marginally resolved by this grid, especially for the smaller friction values ($\epsilon = 0.02$ at the boundary); this issue is discussed further below.

3. Qualitative features of thermocline structure

For the fixed parameter values given above, and for other similar values, the numerical solutions obtained with ϵ, $\kappa_h \leq 0.1$ and $\kappa_v \leq 0.01$ have a similar qualitative three-dimensional thermal structure. In this section, we summarize this structure for a solution with $\epsilon = 0.02$, $\kappa_v = 0.005$ (0.25 cm^2 s^{-1}), $\kappa_h = 0.04$ (2×10^6 cm^2 s^{-1}), $\delta_E = 0.005$ (25 m), $w_{E0} = 1$ (10^{-4} cm s^{-1}), $\gamma_{Ts} = 5$ (0.4 m day^{-1}), and imposed air temperature $T_s = 200$ $(1 - y)$ (dimensional gradient 17 K/5000 km).

The barotropic circulation (as indicated by the depth-integrated pressure P) is anticyclonic in the subtropical gyre between the latitudes $y = 0.25$ and $y = 0.75$, where the Ekman pumping vanishes, and cyclonic in the tropical upwelling region south of $y = 0.25$ and in the subpolar gyre north of $y = 0.75$ (Fig. 2). The Ekman layer temperature T_E is nearly equal to the imposed air temperature T_s except along the western boundary, where warm water is advected northward by the western boundary current and then eastward into

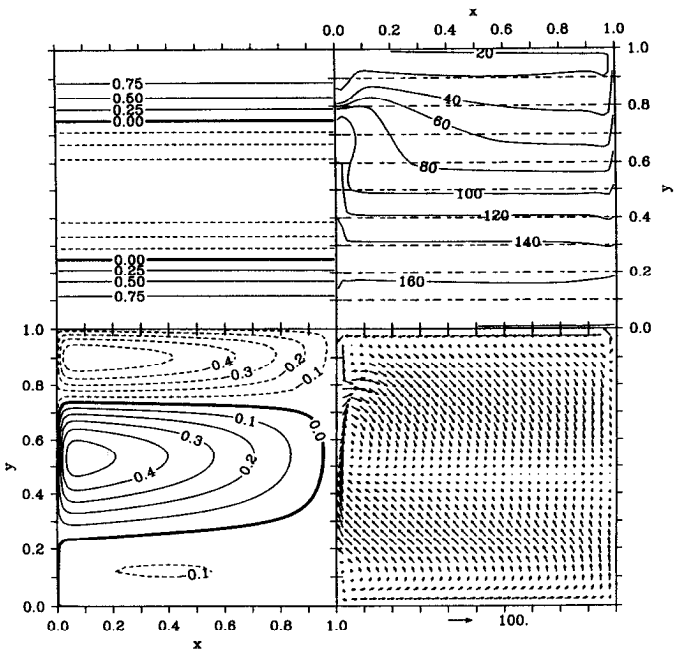

Figure 2. Surface layer variables for the solution described in the text. Clockwise from upper left: (a) Ekman pumping velocity w_E, (b) surface layer temperature T_E (solid contours) and imposed air temperature T_s (dashed contours, contour interval 20), (c) surface boundary layer horizontal velocities (u_A, v_A), (d) barotropic pressure P.

the interior, and along the southern boundary, where it is cooled by upwelling. The near-surface circulation is dominated by a broad anticyclonic baroclinic gyre, which is an order of magnitude stronger than the barotropic gyre, and overflows the latitudes of zero Ekman pumping to the north and south (Fig. 3a). The abyssal circulation forms a weak basin-wide cyclonic gyre closed by westward flow near the northern boundary and southward flow in a western boundary current (Fig. 3b).

Vertical profiles of temperature T, vertical temperature gradient T_z, and vertical velocity w in the center of the subtropical gyre, at $(x, y) = (0.5, 0.5)$, show several distinct regimes (Fig. 4). An isothermal abyss extends from the bottom to roughly $z = 0.75$ (1250 m depth). A sharp maximum in T_z is centered near $z = 0.85$ (750 m). Above the maximum is a secondary isothermal layer and an associated local minimum in T_z. Above this minimum is a second strongly stratified region, with a second maximum in T_z at the surface. Thus, above the nearly homogeneous abyss there are two clearly distinct 'thermoclines' separated by a thin shallow thermostad. We argue below that these two thermoclines are structurally different, in that they arise in two different dynamic regimes. The appearance of these two dynamical thermocline regimes in the limit of small diapycnal diffusion is fundamental, regardless of the number of maxima that arise in the vertical profile of vertical temperature gradient T_z.

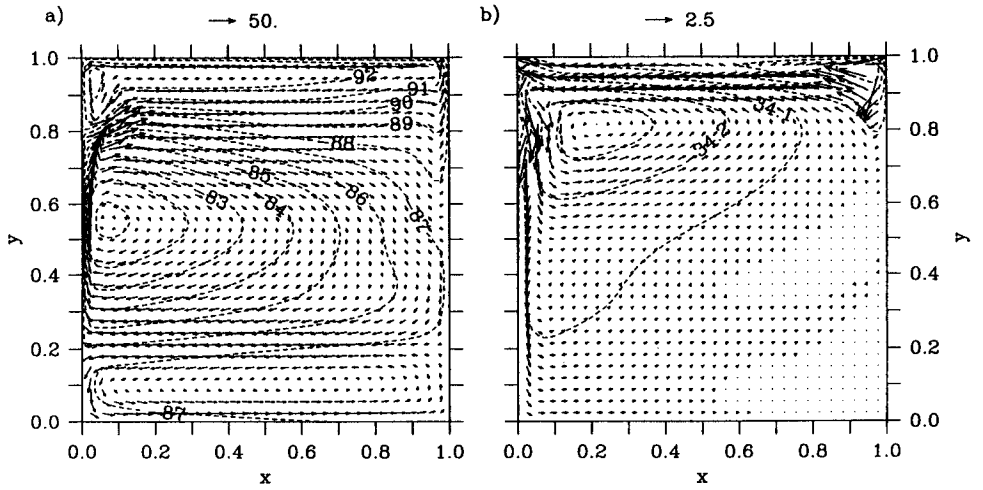

Figure 3. Contours of pressure p and vectors of horizontal velocity (u, v) at (a) the uppermost interior grid level $z = 1$ (at 25 m, the base of the surface boundary layer) and (b) at the grid level $z = 0.69$ (1590 m) for the solution in Figure 2.

The 'two-thermocline' structure extends across most of the subtropical gyre (Fig. 5). The stratification in the upper thermocline weakens toward the northwest. North and south of the subtropical gyre, where the Ekman vertical velocity is upward, a different vertical structure arises. In the north, the abyssal thermostad extends upward to the surface. In the south, the two thermoclines merge into a single surface thermocline, which weakens rapidly with depth. The temperature in the abyssal thermostad is horizontally uniform, whereas the temperature in the shallow subtropical thermostad has significant horizontal gradients (Fig. 5a).

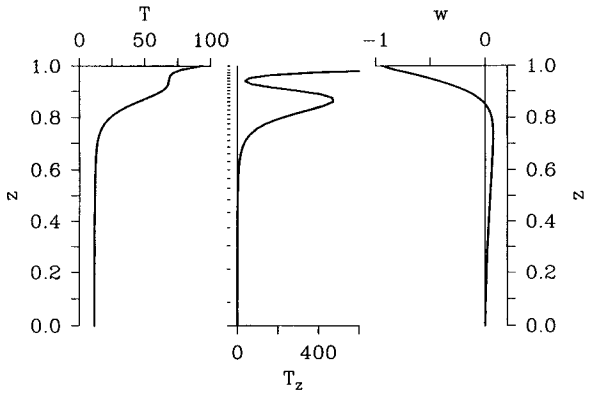

Figure 4. Vertical profiles of T (left panel), T_z (center), and w (right) at the center of the domain, $(x, y) = (0.5, 0.5)$, for the solution in Figure 2.

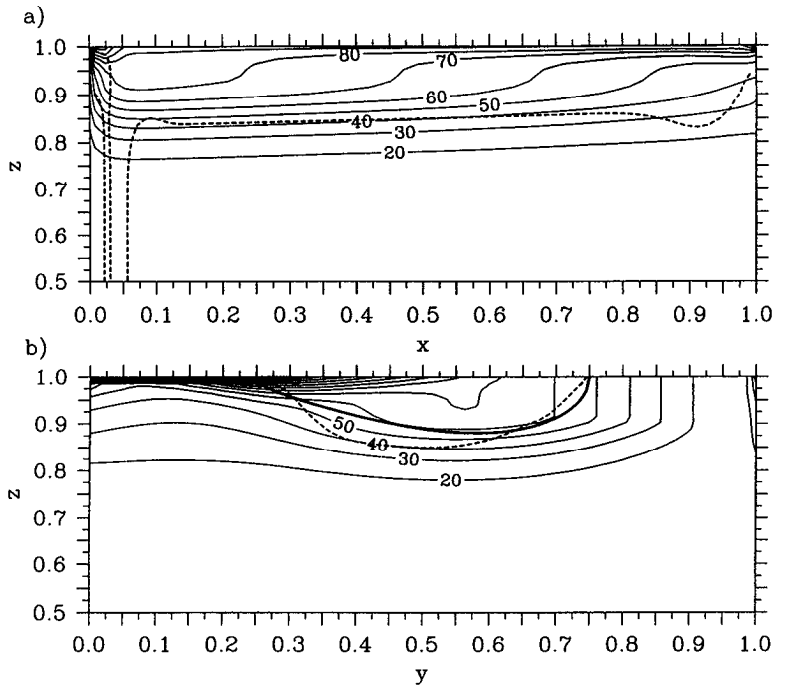

Figure 5. (a) Zonal and (b) meridional cross-sections of temperature T for the solution in Figure 2. Only the upper half of the domain is shown; the deeper fluid is nearly homogeneous. The depth at which $w = 0$ in the subtropical gyre is shown (dashed line), and in (b) the advective scale estimate of thermocline depth, D_a, is also shown (thick line).

Most isopycnal surfaces in the internal thermocline, that is, those close to the internal maximum in T_z, outcrop into the surface mixed layer north of the latitude where the Ekman vertical velocity vanishes (Fig. 6b). The surface maximum in T_z and the shallow thermostad are found on 'ventilated' isopycnal surfaces that outcrop in the subtropical gyre (Fig. 6a). On the surfaces that outcrop in the northern part of the subtropical gyre, the fluid parcel trajectory that is tangent to the outcrop forms a boundary on the isopycnal surface between a ventilated regime to the east, and a recirculation regime to the west. The isopycnal surface descends from east to west through the thermostad across this trajectory, and the recirculation forms part of the internal thermocline. The boundary between these regimes is marked by a tightly packed set of depth contours in Figure 6a. On ventilated trajectories, the fluid parcel density and potential vorticity are effectively set in the mixed layer, nearly conserved in the interior, and then reset by surface cooling as the parcel passes through the western boundary layer and back into the interior. With $\kappa_h = 0.04$ as here, parcel density is partially modified by horizontal diffusion in the boundary layer. In solutions with smaller horizontal diffusivity ($\kappa_h = 0.002$, Section 6, Fig. 14), the western boundary current is nearly adiabatic, and density is reset as the parcel crosses the isopycnal outcrop into the convectively-adjusting mixed layer. Potential vorticity is altered both by

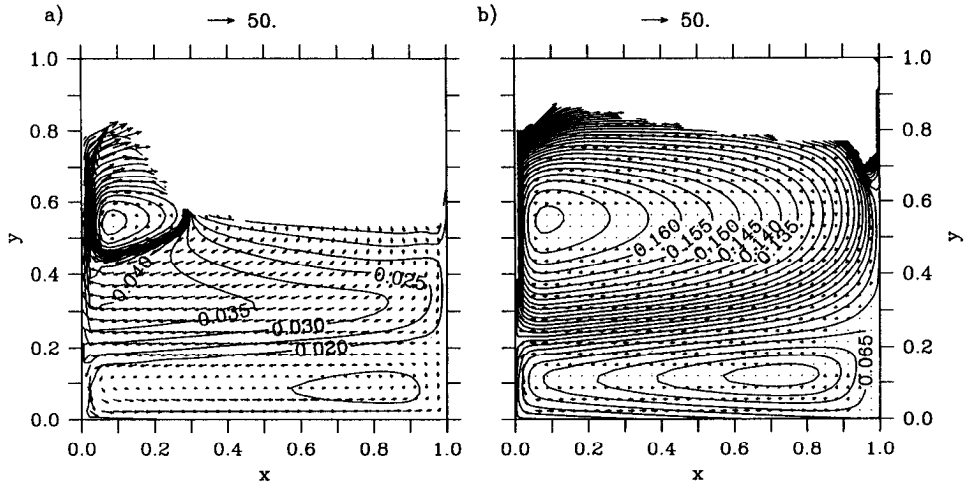

Figure 6. Depth $h = 1 + \delta_E - Z_T$ and vectors of horizontal velocity (u, v) on the isopycnal surfaces $z = Z_T$, (a) $T = 80$, (b) $T = 40$ for the solution in Figure 2. (Dimensional units of 5000 m and 0.1 cm s^{-1}.)

friction in the boundary layer and by the diabatic processes. On recirculating trajectories, the fluid parcels pass through the western boundary layer and return to the interior without entering the mixed layer, and so remain isolated from effective contact with the surface forcing.

The two subtropical gyre thermoclines are the signatures of the two fundamentally different dynamical regimes. The surface maximum in T_z occurs on the ventilated portions of the isopycnal surfaces that outcrop in the subtropical gyre, where the downward vertical velocity is large (Fig. 4). In this regime, the heat balance is advective (adiabatic): the horizontal and vertical advection terms are comparable in size, and larger than the diffusive terms (Fig. 7). The internal maximum in T_z occurs near the zero crossing of the vertical velocity (Fig. 4). In this regime, the heat balance is advective-diffusive (diabatic): the advective and diffusive terms are comparable in size. On the recirculating (unventilated) portions of the ventilated isopycnal surfaces, the heat balance is advective-diffusive, as in the rest of the internal thermocline. The heat balance in the internal thermocline is examined in more detail below (Section 6).

In the tropical region, fluid on ventilated isopycnals upwells into the surface boundary layer, where it gains heat and is driven northward and eventually downward along shallower ventilated isopycnals by Ekman drift and downwelling (Fig. 2, Fig. 6a, Fig. 8). This gain of heat in the ventilated thermocline is compensated in the steady state by heat loss in the northwest corner of the subtropical gyre (Fig. 8). In this region, a deep surface mixed layer forms by convective adjustment. The surface mixed layer deepens eastward along the subtropical-subpolar gyre boundary. At each longitude, the deepest mixed layers are found near $y = 0.95$ in the subpolar gyre, and abyssal convection occurs at a single grid

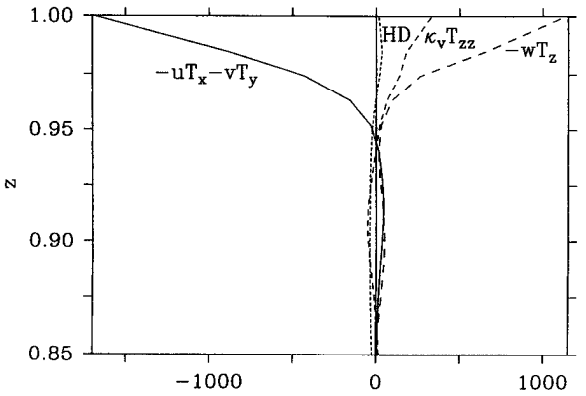

Figure 7. Vertical profiles of terms in the thermodynamic equation for $0.85 < z < 1$ at the center of the domain, $(x, y) = (0.5, 0.5)$, for the solutions in Figure 2. The profiles for horizontal advection $(-uT_x - vT_y)$, vertical advection $(-wT_z)$, vertical diffusion $(\kappa_v T_{zz})$, and horizontal (Laplacian plus biharmonic) diffusion (HD) are labeled. The units are $T*/t* = 5.4 \times 10^{-4}$ K yr^{-1}.

point near the northwest corner of the basin (Fig. 8). Along the eastern part of the gyre boundary, convection is mechanically driven, as cool surface boundary layer fluid is advected southward over warmer interior fluid by the Ekman flow. The dimensional northward heat flux reaches only 10^{14} W, an order of magnitude smaller than estimates of meridional heat transport in the ocean (Hall and Bryden, 1982).

In the advective regime, potential vorticity $Q = fT_z$ and Bernoulli function $B = p + z\rho = p - zT$ are approximately conserved along particle trajectories, and contours of Q and B are nearly parallel to the flow (Fig. 9). In the recirculation regime, the horizontal gradients of Q

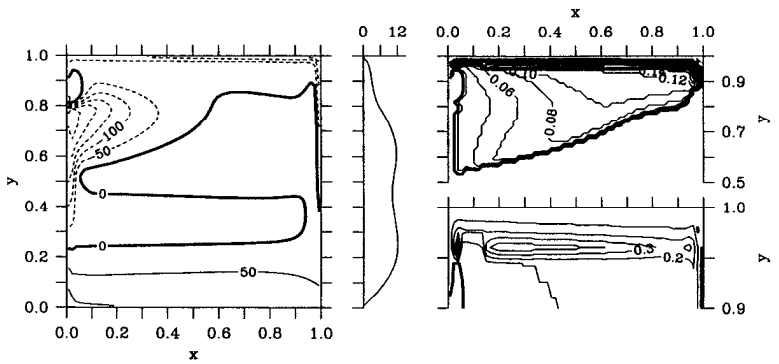

Figure 8. Air-sea heat flux (left panel), zonally-integrated northward ocean heat flux versus latitude y (center), and mixed-layer depth (right) for the solution in Figure 2. The mixed-layer depth for $0 < y < 0.5$ (not shown) is equal to the imposed slab Ekman layer depth δ_E. The lower right panel is an expanded view of the upper right panel for $0.9 < y < 1$. The contour intervals are 50 (17 W m^{-2}) for the left panel, and 0.02 (100 m) and 0.1 (500 m) for the upper and lower right panels, respectively. The dimensional units of zonally integrated heat flux (center panel) are $H_F = 0.9 \times 10^{13}$ W.

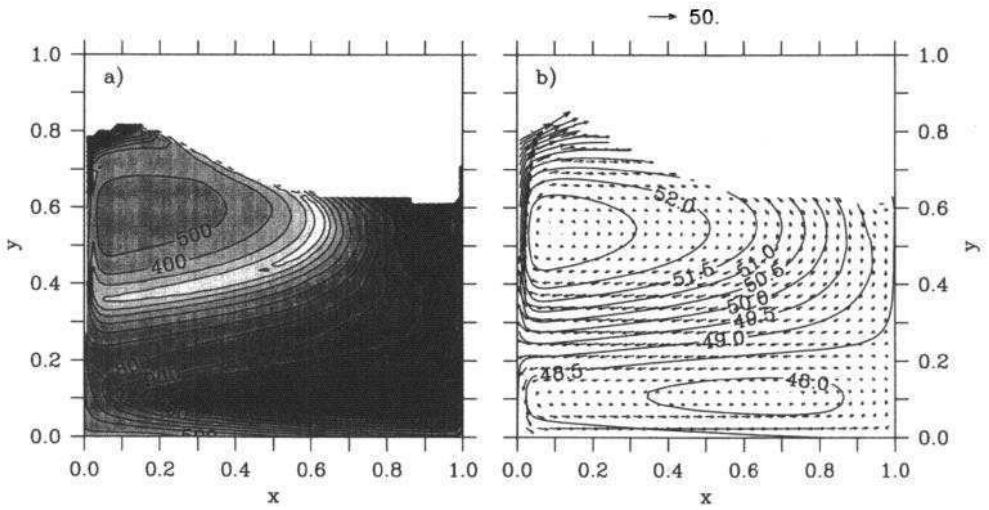

Figure 9. (a) Potential vorticity Q and (b) Bernoulli function B and vectors of horizontal velocity on the $T = 64$ isopycnal surface for the solution in Figure 2.

and B are much weaker than in the advective regime. However, Q and B in this regime are evidently controlled primarily by weak vertical diffusion, rather than horizontal diffusion as in the quasi-geostrophic homogenization theory of Rhines and Young (1982). The concentration of the deep stratification in the internal thermocline, and the attendant absence of a stratified, unventilated regime in which weak horizontal diffusion may dominate weaker vertical diffusion, effectively prevents homogenization by the Rhines-Young mechanism. Note that lateral diffusive effects have been intentionally minimized in the present calculations, by the use of small horizontal diffusivities and the absence of any explicit eddy dynamics; if these effects were restored, a Rhines-Young regime might emerge. The three-dimensional structure of T, and the distribution of Q and B on isopycnals outcropping in the subtropical gyre are qualitatively similar to the corresponding fields from primitive equation solutions in similar idealized geometries with similar numerical grids (e.g., Cox and Bryan, 1984, including coarse-grid results shown only in Cox, 1985, Figures 4–6). This structure is more clearly defined in the present solutions, because of the weaker lateral diffusion.

In the advective-diffusive regime, the solution may be usefully compared with the internal boundary layer equation of Stommel and Webster (1962), and this is done in Section 6. In the advective regime, the solution may be usefully compared with the ventilated thermocline layer-model solutions of Luyten *et al.* (1983), and this is done in Section 7. The flow in the abyssal thermostad is driven by relatively uniform interior upwelling (Fig. 10), and so (by Sverdrup balance) is northward in the interior, toward the northern source of deep water, essentially as in the theory of Stommel and Arons (1960). A similar division of the interior flow into ventilated, advective-diffusive, and abyssal regimes was found in a planetary geostrophic model by Colin de Verdiere (1989), while

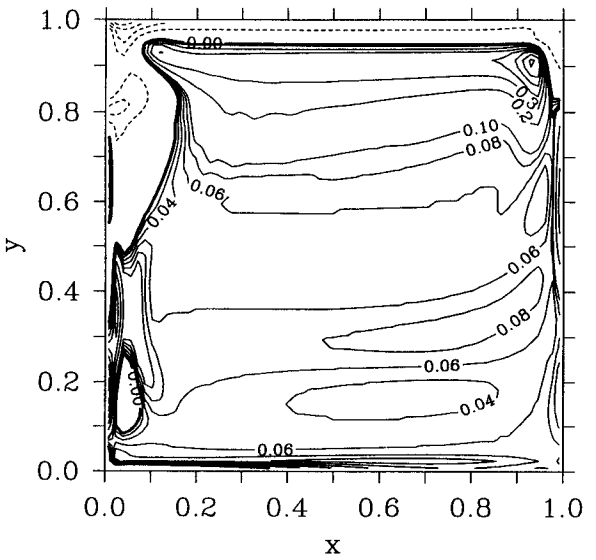

Figure 10. Vertical velocity w at the level $z = 0.65$ (1750 m) for the solution in Figure 2. The contour intervals for w are 1 (10^{-4} cm s^{-1}) for $w < 0$, 0.02 for $0 < w < 0.1$, and 0.1 for $w > 0.1$.

Salmon (1990) focused on the internal thermocline; the smaller diffusion coefficients used in the present calculations result in a more complete separation of these regimes, and allow a more direct comparison with thermocline theories.

4. Scaling: the two-thermocline limit

a. Thermocline scaling. The vertical temperature gradient T_z in the solution described above has two well-defined maxima in the subtropical gyre, one at the surface, and one near the zero-crossing of the vertical velocity. In order to understand how these maxima are maintained, it is useful to recall the scaling argument that Welander (1971b) used to infer the presence of an adiabatic thermocline regime, and then to extend part of this argument in a simple way. These scaling arguments compactly describe the essential physics of the quantitative theories that we consider in the succeeding sections.

Consider the case in which the vertical velocity is internally determined, with advection and vertical diffusion both entering the thermodynamic balance, so that in the thermocline the terms in the thermal wind, continuity, and thermodynamic equations, respectively, may be estimated as

$$fU/\delta \sim g\alpha\Delta T_d/L \tag{4.1}$$

$$U/L \sim fW_d/\delta \tag{4.2}$$

$$U\Delta T_d L,\ W_d\Delta T_d/\delta \sim \kappa\Delta T_d/\delta^2 \tag{4.3}$$

Here ΔT_d is a scale for horizontal variations in temperature over the gyre scale L. We take

$L \sim f/\beta$, so that no independent scaling may be derived from the vorticity balance, and horizontal and vertical advection are of the same order. (A reviewer has pointed out that if separate estimates of gyre scale L and planetary scale f/β are retained in the case of the advective scale described below, the resulting scaling gives information on the amount of recirculation within the gyre (Rhines and Young, 1982). We persist with the simpler $L \sim f/\beta$ scaling here, as it is adequate to our purposes, but its limitations should be recognized.) This scaling has been termed the 'advective-diffusive' balance (Welander, 1971b). With the parameters f, g, α given, these relations may be solved for δ, W_d, and U in terms of κ to yield

$$\delta \sim (\kappa f L^2/g\alpha\Delta T_d)^{1/3} \propto \kappa^{1/3} \tag{4.4}$$

$$W_d \sim \kappa/\delta \propto \kappa^{2/3} \tag{4.5}$$

$$U \sim \kappa L/\delta^2 \tag{4.6}$$

For $f = 10^{-4}\ \mathrm{s}^{-1}$, $\beta = 2 \times 10^{-13}\ \mathrm{cm}^{-1}\ \mathrm{s}^{-1}$, $f/\beta \sim L = 5 \times 10^8$ cm, $g = 980\ \mathrm{cm\ s}^{-2}$, $\alpha = 10^{-4}\ \mathrm{K}^{-1}$, $\Delta T_d = 10$ K, and $\kappa = 0.1\ \mathrm{cm}^2\ \mathrm{s}^{-1}$, this gives $\delta \sim 130$ m, $U \sim 0.3\ \mathrm{cm\ s}^{-1}$, and $W_d \sim 10^{-5}\ \mathrm{cm\ s}^{-1}$.

In the central subtropical gyre, the downward Ekman pumping velocity W_E is much greater than this advective-diffusive estimate of the vertical velocity ($W_E \sim 10^{-4}\ \mathrm{cm\ s}^{-1} \gg W_d$). Consequently, vertical advection overwhelms vertical diffusion near the surface, and an advective balance must result in the thermodynamic equation (Welander, 1971b). In this case (which then should apply on ventilated isopycnal surfaces in the upper subtropical gyre in the solution discussed above), the scaling relations become

$$fV/D_a \sim g\alpha\Delta T_a/L \tag{4.7}$$

$$V/L \sim W_E/D_a \tag{4.8}$$

$$V\Delta T_a/L \sim W_E\Delta T_a/D_a, \tag{4.9}$$

where now the thermodynamic scale balance is also redundant and may be dropped. This scaling has been termed the 'advective' balance (Welander, 1971b). With W_E given, these relations yield

$$D_a \sim (W_E f L^2/(g\alpha\Delta T_a))^{1/2} \tag{4.10}$$

$$V \sim W_E L/D_a \tag{4.11}$$

For the above values, and with $\Delta T_a = \Delta T_d = 10$ K, $D_a \sim 400$ m and $V \sim 1\ \mathrm{cm\ s}^{-1}$.

The advective scaling for the vertical derivative of the vertical velocity is consistent with the vanishing of the vertical velocity at depth D_a, so the advective scale D_a has a natural interpretation as the thickness of the fluid layer that is set in motion by the wind. If the wind-driven vertical velocity vanishes at the advective depth D_a, then near that depth it will be negligible relative to the small, but finite, internally-determined velocity W_d derived

from the advective-diffusive scaling, no matter how large W_E is at the surface. Thus, it is natural to anticipate that an advective-diffusive regime may exist beneath the advective regime (Welander, 1971b). The vertical scale δ might then apparently describe the thickness of an advective-diffusive thermocline near depth D_a.

Salmon (1990) suggested that the ocean thermocline could be identified as an advective-diffusive regime that arises as an 'internal boundary layer' in this manner. However, he argued that the vertical scale describing this regime was not the advective-diffusive depth $\delta \sim \kappa_v^{1/3}$ but instead should be proportional to $\kappa_v^{1/2}$, as in a similarity solution discussed by Stommel and Webster (1962) and Young and Ierley (1986). The modified advective-diffusive 'internal boundary layer' vertical scale may be obtained by a simple extension of the scaling arguments above, following the idea that 'the isotherms near the thermocline all had a constant but undetermined slope' (Stommel and Webster, 1962, p. 55). For sufficiently small κ_v, $\delta \ll D_a$. In this case, the advective-diffusive estimate of the horizontal temperature gradient in the thermal wind balance (4.1) must be modified: rather than the gyre scale, the appropriate horizontal scale for the estimate of the horizontal temperature gradient in the thermal wind relation is the horizontal distance across the thermocline itself. This is given by the diffusive thermocline thickness δ_i divided by the (advective) aspect ratio D_a/L, so that

$$fV/\delta_i \sim g\alpha\Delta T_i/(\delta_i L/D_a) \tag{4.12}$$

$$V/L \sim W_i/\delta_i \tag{4.13}$$

$$W_i\Delta T_i/\delta_i \sim \kappa\Delta T_i/\delta_i^2 \tag{4.14}$$

where ΔT_i is the temperature difference across the thermocline. This is equivalent, for a given wind forcing, to fixing the slope of the isotherms, since the unknown thickness δ_i cancels out of the scaled thermal wind balance. From a physical point of view, the isotherm slopes are effectively fixed because the weak vertical diffusion can move isotherms vertically by only a small fraction of their large-scale deviation from horizontal, which is controlled by the wind-forcing and measured by D_a. Since the thermal wind balance is independent of δ_i, the velocity scale V is the advective velocity $W_E L/D_a$ (taking $\Delta T_a \sim \Delta T_i$ here for simplicity), while W_i and δ_i are given by

$$\delta_i \sim (\kappa f L^2/(g\alpha\Delta T_i D_a))^{1/2} \sim (\kappa(fL^2/(g\alpha\Delta T_i W_E))^{1/2})^{1/2} \propto \kappa^{1/2} \tag{4.15}$$

$$W_i \sim \kappa/\delta_i \propto \kappa^{1/2}. \tag{4.16}$$

This third depth scale δ_i, which is an advective-diffusive scale, may be termed the 'internal boundary layer' scale, to distinguish it from the conventional advective-diffusive scale δ. An internal boundary layer that obeys this scaling has been found previously by Stommel and Webster (1962) and Young and Ierley (1986) in a similarity solution of the thermocline equations.

Welander (1971b) showed that the advective and advective-diffusive scales may be

derived either in terms of the fundamental physical balances as here, or by direct consideration of the scalar form of the thermocline equations corresponding to (2.17) with $\epsilon = \kappa_h = \lambda = 0$. In the latter case, the internal boundary layer scale arises if the horizontal derivative in the term $M_x M_{zzz}$ is estimated as a vertical derivative times a fixed slope, consistent with the similarity form considered by Stommel and Webster (1962).

Thus, in the limit of small diapycnal diffusion, the advective scale D_a characterizes the depth to which the wind-driven motion extends, and the internal boundary layer scale δ_i characterizes the thickness of the thermocline that forms at the base of the wind-driven fluid layer. In order to evaluate the expressions for D_a and δ_i, it is necessary to choose values for the temperature scales ΔT_a and ΔT_i. Beneath the internal boundary layer, the abyssal ocean fills with the densest fluid, with temperature characterized by the coldest air temperature, which is found at the northern edge of the subpolar gyre. The surface temperature in the subtropical gyre depends on the balance between surface thermal forcing and horizontal advection. If ΔT_s and ΔT_E characterize the air temperature forcing and the Ekman layer temperature variations in the subtropical gyre, respectively, then the terms in the Ekman layer heat balance may be estimated as

$$(V + V_E)\Delta T_E/L \sim (\Delta T_s - \Delta T_E)/t_E \tag{4.17}$$

which may be solved for ΔT_E to yield

$$\Delta T_E \sim \Delta T_s/(1 + (V + V_E)t_E/L) \tag{4.18}$$

where $V_E \sim LW_E/\delta_E$ is the horizontal Ekman velocity scale for an Ekman layer of depth δ_E, and $t_E = \delta_E/\gamma_{Is}$ is a relaxation time scale from the thermal forcing for the Ekman layer temperature. If the relaxation time scale is shorter than the advective time scales, the temperature in the Ekman layer will be approximately equal to the local air temperature. For the dimensional values given above, with $\delta_E = 25$ m, the advective time scales are ~9 months for the Ekman advection and ~24 years for the geostrophic advection, significantly larger than a typical relaxation time scale $t_E \sim 25$ m/0.4 m day$^{-1} \sim 2$ months. Thus, the surface temperature in the interior of the subtropical gyre may be estimated directly from the local air temperature. (This is not true in the northwest part of the gyre, where advection by the western boundary current has a timescale comparable to or shorter than the relaxation time scale.) Then the temperature of the deepest wind-driven fluid can be estimated from the air temperature at the subtropical-subpolar gyre boundary, where the downward Ekman pumping vanishes (again neglecting the warming due to northward advection by the western boundary current). Consequently, to first order the internal thermocline temperature scale ΔT_i can be taken equal to the air temperature difference across the subpolar gyre, ΔT_{SP}, and the advective temperature scale ΔT_a can be taken equal to ΔT_i plus the difference between local air temperature and the air temperature at the subtropical-subpolar gyre boundary, ΔT_{ST}:

$$\Delta T_i \sim \Delta T_{SP} \tag{4.19}$$

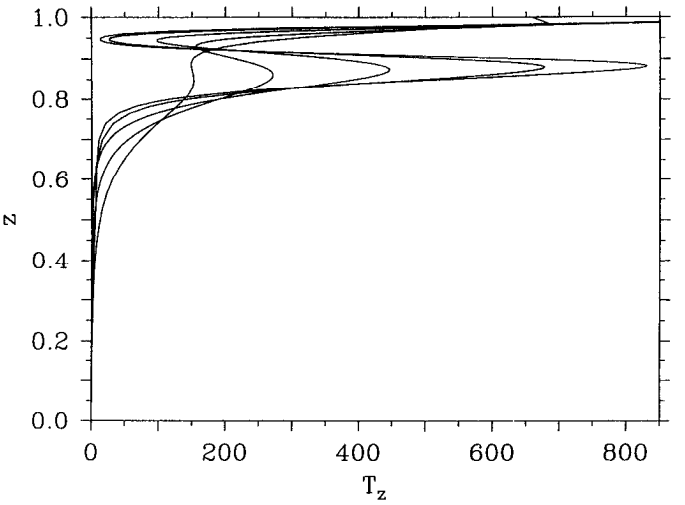

Figure 11. Vertical profiles of T_z at the center of the domain, $(x, y) = (0.5, 0.5)$, for a set of solutions with κ_v = [0.003, 0.004, 0.008, 0.016, 0.032] (0.15, 0.2, 0.4, 0.8, 1.6 $cm^2\ s^{-1}$), $\kappa_h = 0.002$ ($10^5\ cm^2\ s^{-1}$), and $\epsilon = 0.04$. The internal maximum in T_z increases with decreasing κ_v.

$$\Delta T_a \sim \Delta T_{SP} + \Delta T_{ST} \tag{4.20}$$

This closes the scaling theory in terms of the forcing and the given parameters. The qualitative picture that emerges from the scaling, the numerical solutions, and the comparisons with the quantitative theories presented below is illustrated in Figure 1.

b. Numerical results. The parameter dependences derived above from scaling arguments are generally consistent with numerical solutions of the model equations for $\kappa_h \leq \kappa_v \leq 0.01$. The depth and thickness of the internal maximum in T_z may be estimated from vertical profiles of T_z in the center of the subtropical gyre (Fig. 11). The depth of the internal maximum in T_z is independent of κ_v (to first order) as $\kappa_v \to 0$ and proportional to the square-root of the amplitude w_{E0} of the Ekman pumping (Fig. 12), consistent with the scaling for D_a (4.10). The thickness of the internal boundary layer, estimated as the lower half-width at half-maximum of the T_z peak, is proportional to the square-root of κ_v (Fig. 13a), consistent with the scaling for δ_i (4.15). The solution with $\kappa_v = 0.032$ (1.6 $cm^2\ s^{-1}$) has a time-dependent abyssal circulation, but the thermocline depth and thickness are effectively constant.

In order to isolate the effect of the vertical diffusivity, and prevent horizontal diffusion in the western boundary current from overwhelming the interior vertical diffusion (Veronis, 1975), the solutions in Figure 13 have been obtained with $\kappa_h = 0.002$ ($10^5\ cm^2\ s^{-1}$). With this value of horizontal diffusivity, the diapycnal diffusive fluxes through the internal thermocline ($10 < T < 70$) are dominated by vertical diffusion (Fig. 14a). In contrast, for the Case 1 solution above, which has $\kappa_h \gg \kappa_v$ ($\kappa_h = 0.04$, $\kappa_v = 0.005$), the horizontal

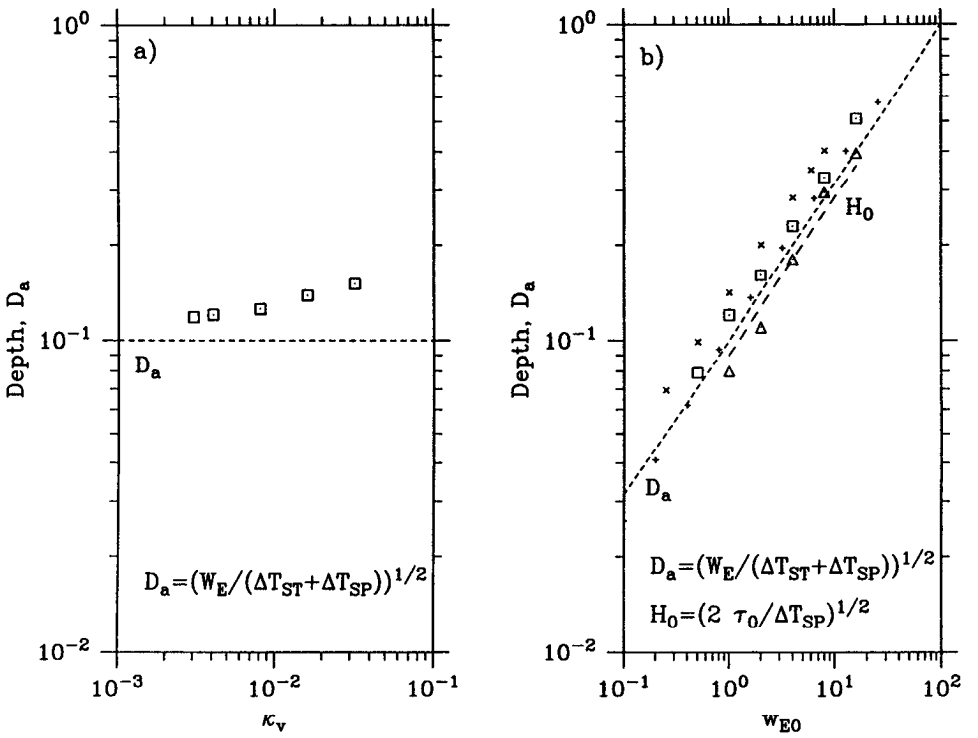

Figure 12. (a) Depth of the internal maximum of T_z (□) versus κ_v, from the profiles in Figure 11. The advective scale depth D_a, which is independent of κ_v, is also shown (dashed line). (b) Depth of the internal maximum of T_z at $(x, y) = (0.5, 0.5)$ (□) and maximum mixed layer depth at the subtropical-subpolar gyre boundary ($y = 0.75$) (△) versus Ekman pumping velocity w_{E0} (10^{-4} cm^2 s^{-1}) for a set of solutions with $\kappa_v = 0.008$ (0.4 cm^2 s^{-1}), $\kappa_h = 0.08$ (4×10^6 cm^2 s^{-1}), $\epsilon = 0.04$. The advective scale depth D_a, which is proportional to the square-root of w_{E0}, is also shown (dashed line), along with the corresponding depths from solutions of the similarity equations (6.1) (×) and (6.2) (+), and the estimate of H_0 from (7.1).

diffusive fluxes through the internal thermocline are comparable to the vertical fluxes (Fig. 14b). Note that there is a small amount of counter-gradient zonal diffusive flux in both cases due to the biharmonic diffusion. Although this flux is unphysical, it is evidently not pathological as long as it is small relative to the down-gradient flux. The magnitude of the counter-gradient flux can be controlled by adjusting the value of λ. Solutions with λ adjusted to give purely downgradient net flux do not differ substantially from the solutions presented here.

For the solutions in Figure 11 (except the unsteady $\kappa_v = 0.032$ case), the corresponding profiles of vertical velocity in the center of the subtropical gyre have a simple structure, similar to that in Figure 4. The magnitude of the downward vertical velocity decreases linearly from the surface to zero near the maximum in T_z. Beneath this point, it increases to a maximum upward velocity below the internal boundary layer, and then decreases linearly

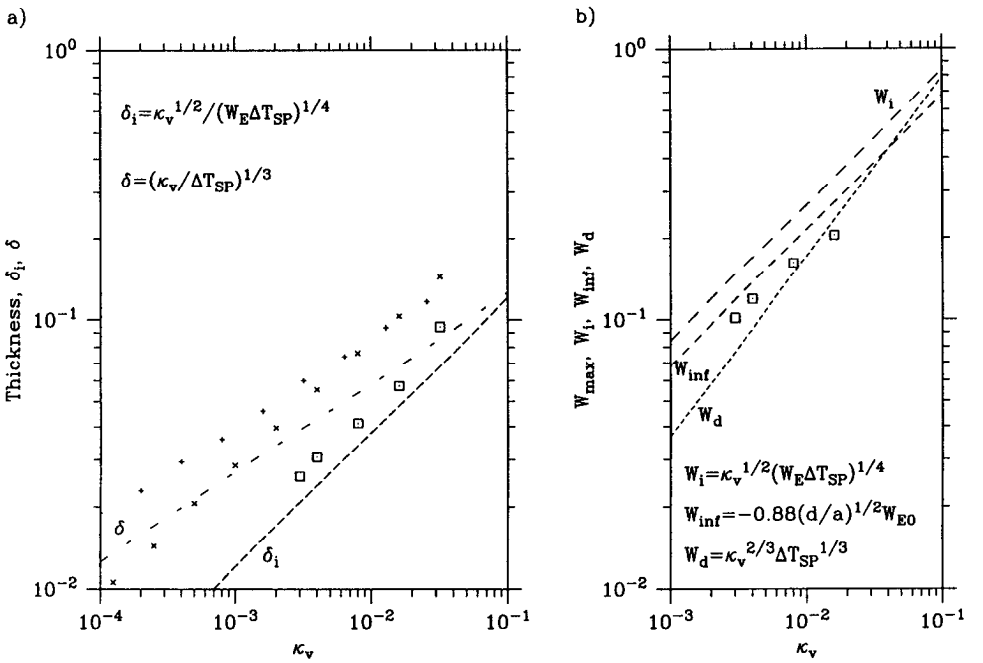

Figure 13. (a) Thickness of the internal peak of T_z (□) versus κ_v, from the profiles in Figure 11. The internal boundary layer scale δ_i and the advective-diffusive scale δ are also shown (dashed lines), along with the corresponding thicknesses from solutions of the similarity equations (6.1) (×) and (6.2) (+). (b) Maximum upward vertical velocity at $(x, y) = (0.5, 0.5)$ versus κ_v, from the solutions in Figure 11. The internal boundary layer scale W_i, the asymptotic estimate $W_{inf} = W_\infty$ from Young and Ierley (1986) for solutions of (6.1), and the advective-diffusive scale W_d are also shown (dashed lines).

through the isothermal abyss to zero at the bottom. The maximum upward velocity is proportional to the square-root of κ_v (Fig. 13b), consistent with the scaling for W_i [see (4.16)]. For the smallest values of κ_v, the upward abyssal w does not always penetrate to the bottom, as the horizontal diffusion is sometimes sufficient to damp the deep flow, despite the small value of κ_h.

In the central subtropical gyre, the dependence on κ_v of the amplitude of the zonally-integrated meridional overturning stream function ψ is roughly consistent with the internal boundary layer scaling for W_i, where the scaling estimate of the stream function is $M \sim W_i L^2$ (Fig. 15). This is effectively an integrated test of the scaling for W_i, and is consistent with the hypothesis that the overturning in the central subtropical latitudes is controlled by vertical diffusive fluxes in the interior, not horizontal diffusive fluxes across the western boundary current. To the north and south, the dependence of ψ on κ_v is sharper, so that $\psi_{max} \sim \kappa_v^{2/3}$ for both the subtropical gyre and the full basin, in agreement with the form (but not the numerical value) of the dependence that would be predicted by the advective-diffusive scaling (4.5). Note that the zone of tropical upwelling may be unrealistically large

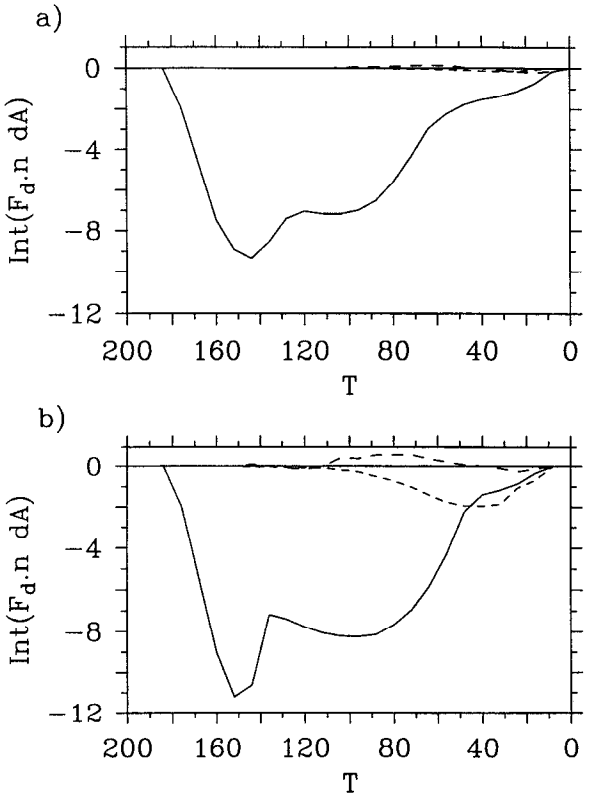

Figure 14. Diffusive fluxes through isopycnal surfaces (diapycnal fluxes) from vertical (solid line), zonal (long dashes), and meridional (short dashes) diffusion versus temperature for (a) the solution with $\kappa_v = 0.003$ in Figure 11 and (b) the solution in Figure 2. The sign convention is negative downgradient, and the T-axis is reversed so that density increases to the right. The units of heat flux are $H_F = 0.9 \times 10^{13}$ W.

in the present calculation because of the form (2.22) of the imposed Ekman pumping, possibly exaggerating the influence on the meridional overturning stream function of diffusion in the shallow tropical thermocline. We do not attempt a complete analysis of the meridional overturning circulation here.

These scaling results may be compared with those obtained by Bryan (1987) from primitive equation calculations on a $17 \times 21 \times 12$ spherical grid in a basin of similar size, forced by fixed wind-stress and Newtonian heat and salt fluxes. Note that the horizontal temperature diffusivity for most of those calculations was (with the present nondimensionalization) $\kappa_h = 0.2$ (10^7 cm^2 s^{-1}), 100 times larger than for the solutions in Figure 11. Bryan (1987) found that both thermocline thickness and meridional overturning stream function scaled approximately as $\kappa_v^{1/3}$. In the present case, we find a stronger ($\kappa_v^{1/2}$, $\kappa_v^{2/3}$) dependence on vertical diffusivity. Bryan also found that thermocline depth increased with

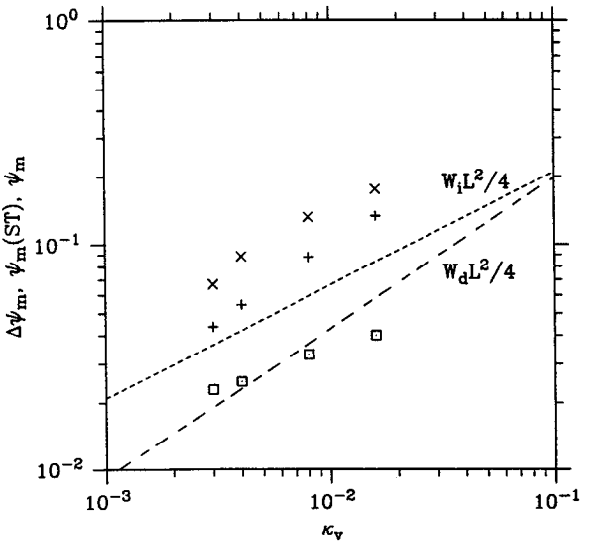

Figure 15. Amplitude of meridional overturning stream function ψ (stream function of zonally averaged circulation) versus κ_v for the solutions in Figure 11. The change in amplitude (□) over the central subtropical gyre (between $y = 0.375$ and $y = 0.625$), where the maximum over depth z is taken excluding the shallow tropical wind-driven cell, and the the subtropical gyre (+) and full-basin (×) maxima are shown. The dashed lines show estimates based on the internal boundary layer (W_i) and advective-diffusive (W_d) vertical velocity scales.

wind forcing, in accordance with our results, but did not evaluate this dependence quantitatively. Winton (1995, 1996) has found $\kappa_v^{1/2}$ and $\kappa_v^{1/3}$ scalings for meridional overturning in planetary geostrophic models with two and three spatial dimensions forced only by surface buoyancy fluxes.

5. Dependence on structure of meridional air temperature

According to the internal boundary layer scaling, the diapycnal upwelling velocity at the base of the internal thermocline depends on the temperature difference across the internal thermocline, which to first order may be taken equal to the air temperature difference across the subpolar gyre. Consequently, the meridional overturning cell associated with upwelling in the internal thermocline depends to first order on the air temperature gradient across the subpolar gyre, not the gradient across the entire domain. This dependence may be explicitly demonstrated by examining the thermocline structure and overturning circulation in a solution (Case 1A) identical to that discussed above (Case 1), but with uniform air temperature from the southern boundary to the subtropical-subpolar gyre boundary.

The internal thermocline structure for Case 1A (Fig. 16a) closely resembles that for Case 1 (Fig. 5b). The temperature difference across the internal thermocline in Case 1A is somewhat less than that in Case 1, since northward advection in the western boundary

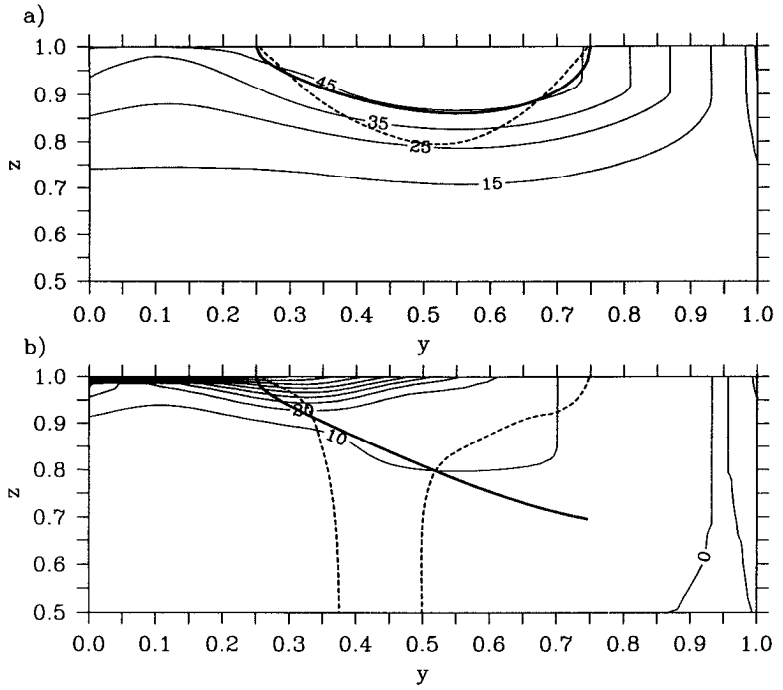

Figure 16. Meridional cross-sections of temperature T at $x = 0.5$ for (a) a solution with air temperature T_s constant for $y \leq 0.75$, (b) a solution with air temperature T_s constant for $y \geq 0.75$. Only the upper half of the domain is shown; the deeper fluid is nearly homogeneous. The depth at which $w = 0$ in the subtropical gyre is shown (dashed line), along with the corresponding advective scale estimate D_a of thermocline depth (thick line).

current and direct contact between the atmosphere and the internal thermocline in the deep mixed layer of the western boundary current outflow supply warmer fluid to the top of the internal thermocline in Case 1. The meridional overturning stream functions for Case 1 and Case 1A are nearly identical in structure and amplitude (Fig. 17a,b). This illustrates directly that for small diapycnal diffusion, the meridional overturning circulation (which is driven by vertical diapycnal diffusion through the internal thermocline) is effectively insulated from the surface thermal forcing in the subtropical gyre by the circulation associated with the ventilated thermocline.

The thermocline structure and meridional overturning stream function for the complementary Case 1B, for which the air temperature is identical to that of Case 1 south of the subpolar gyre boundary but uniform across the subpolar gyre, differs substantially from that for Case 1 and Case 1A (Figs. 16b, 17c). Case 1B has a ventilated thermocline regime, near the surface in the subtropical gyre, but only a weak remnant of the internal thermocline. The meridional overturning cell is weak and broad, filling the entire abyss.

These cases illustrate directly that for small diapycnal diffusion, the internal thermocline depends strongly on the thermal forcing across the subpolar gyre, but only weakly on that

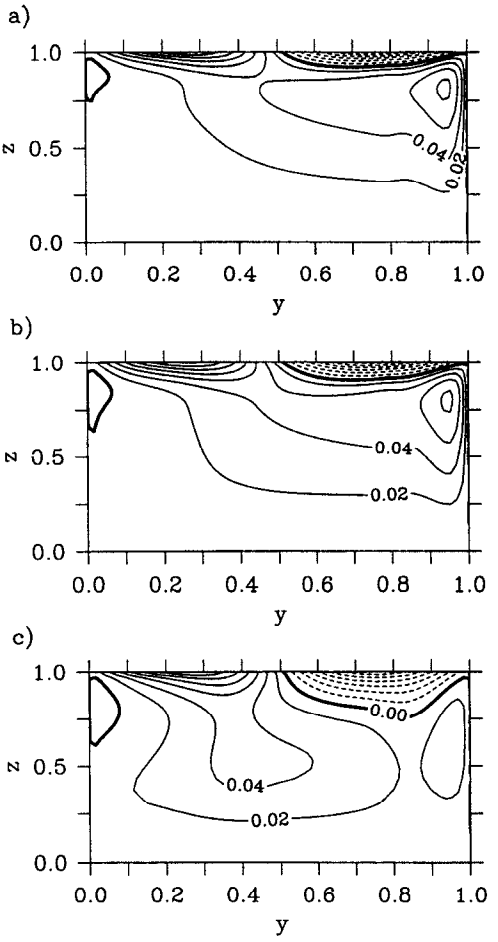

Figure 17. Meridional cross-sections of meridional overturning stream function ψ for the solutions in (a) Fig. 2, (b) Fig. 16a, (c) Fig. 16b. The sense of the circulation is clockwise around maxima in ψ.

across the subtropical gyre, while the structure of the ventilated thermocline is only weakly dependent on the forcing in the subpolar gyre. The advective scale (4.11), with the temperature scale ΔT_a chosen according to (4.20), gives a useful estimate of the mid-basin depth of the internal thermocline in all three cases (Fig. 5b, Fig. 16).

6. Comparison with the internal boundary layer theory

a. Numerical results. The numerical results above indicate that the dependence of internal thermocline thickness on vertical diffusivity is consistent with the internal boundary layer scaling that arises in the similarity solutions of the thermocline equations studied by Stommel and Webster (1962) and Young and Ierley (1986). This motivates the quantitative

comparison of the current results with the similarity solutions. We focus on the vertical-diffusive control of the structure of the thermocline in the central subtropical gyre.

A nonlinear ordinary differential equation whose solutions exhibit the internal boundary layer scaling for thermocline thickness was proposed by Stommel and Webster (1962) as an *ad hoc* simplification of a similarity form obtained by Robinson and Stommel (1959) for the thermocline equations. This equation, which has been derived more rigorously from a more general similarity form by Young and Ierley (1986), may be written

$$\left(2\tilde{W} - \zeta \frac{d\tilde{W}}{d\zeta}\right) \frac{d^3\tilde{W}}{d\zeta^3} = \kappa_v \frac{d^4\tilde{W}}{d\zeta^4} \tag{6.1}$$

where $\zeta = (z - 1)/(1 - x)^{1/3}$ is a similarity variable, the vertical velocity is $w = (1 - x)^{-1/3}(2\tilde{W} - \zeta d\tilde{W}/d\zeta)$, and the temperature is $T = -3(f^2/\beta)d^2\tilde{W}/d\zeta^2$. The dependence of T on ζ fixes the slope of the isotherms, and in solutions of this equation with downward vertical velocity (Ekman pumping) imposed at the surface ($w < 0$ at $\zeta = 0$), the thickness of the thermocline that forms near the zero-crossing of the vertical velocity obeys the internal boundary layer scaling $\delta_i \sim \kappa_v^{1/2}$ (Fig. 13). It is instructive to consider also the simpler equation proposed by Salmon (1990) as a model for the internal boundary layer,

$$\hat{W} \frac{d^3\hat{W}}{dz^3} = \kappa_v \frac{d^4\hat{W}}{dz^4} \tag{6.2}$$

where the vertical velocity is $w = \hat{W}$ and the temperature is $T = (f^2/\beta)(1 - x)d^2\hat{W}/dz^2$. In this case, the isotherm slopes are not known until the differential equation for $\hat{W}$ is solved. Consequently, the thickness of the thermocline layer that forms in (6.2) in fact obeys the advective-diffusive scaling ($\delta \sim \kappa_v^{1/3}$), not the internal boundary layer scaling ($\delta \sim \kappa_v^{1/2}$). (The Taylor series argument used by Salmon (1990) to infer the internal boundary layer scaling for (6.2) fails because the vertical convergence w_z in the boundary layer depends at lowest order on the boundary layer thickness.)

In the similarity solutions, the horizontal advection of heat vanishes identically, and there is no horizontal heat diffusion, so the balance is between vertical advection and vertical diffusion. In the solutions of the present model with $\kappa_h = 0.002$, the heat balance in the lower half of the internal thermocline is also dominated by a balance between vertical advection and vertical diffusion even for $\kappa_v = 0.003$, the smallest vertical diffusivity considered here (Fig. 18). In the upper half of the internal thermocline, horizontal advection is comparable to vertical advection for $\kappa_v = 0.003$ (Fig. 18a). The relative magnitude of horizontal advection in the internal thermocline decreases as κ_v increases above this value. In the western boundary layer, the local balance is advective in the upper part of the internal thermocline, while horizontal diffusion across the tilted isopycnals of the internal thermocline is large in the lower part (Fig. 18b). This horizontal diffusion is locally several times larger than the dominant terms in the interior, but is not large enough to control the total diffusive flux across the internal thermocline (Fig. 14). (The residual

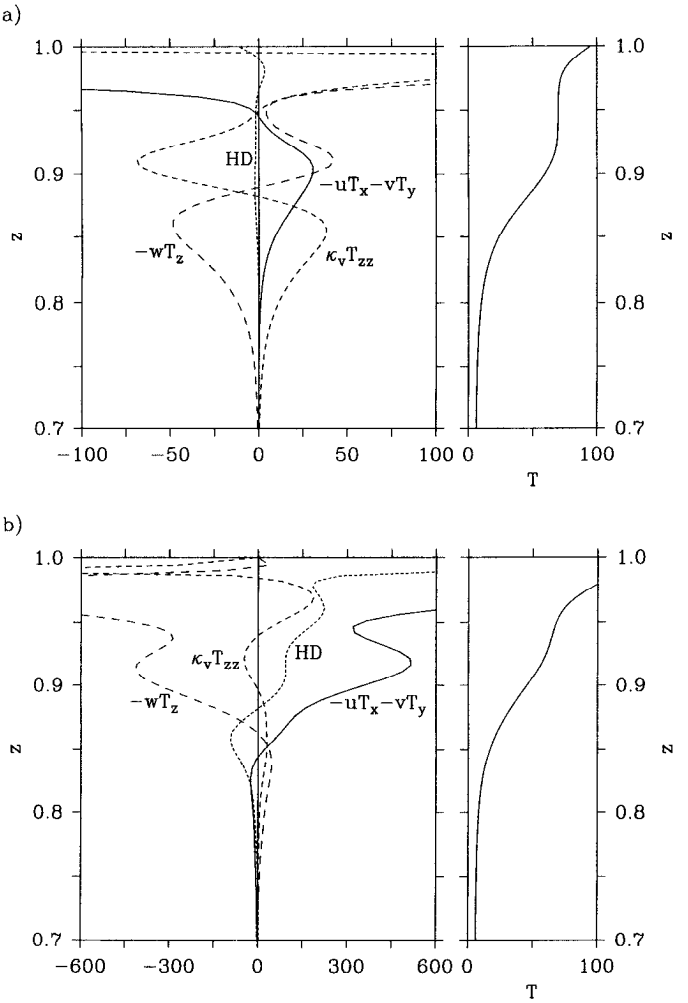

Figure 18. Vertical profiles of terms in the thermodynamic equation for $0.7 < z < 1$ for the solution in Figure 11 ($\kappa_h = 0.002$) with $\kappa_v = 0.003$ at (a) the center of the domain, $(x, y) = (0.5, 0.5)$, and (b) near the western boundary, $(x, y) = (0.024, 0.5)$. The profiles for horizontal advection $(-uT_x - vT_y)$, vertical advection $(-wT_z)$, vertical diffusion $(\kappa_v T_{zz})$, and horizontal (Laplacian plus biharmonic) diffusion (HD) are labeled accordingly. The corresponding profiles of T are also shown (right panels). The units are $T*/t* = 5.4 \times 10^{-4}$ K yr^{-1}.

evident in the lower panel of Figure 18 is a measure of truncation error, as the thermodynamic equation is discretized in flux form. However, improving the horizontal resolution in the western boundary layer does not substantially change these solutions, as discussed below.) The approximate balance of vertical advection and vertical diffusion obtains only in the central subtropical gyre. As the meridional isopycnal slopes increase

toward the northern and southern boundaries of the gyre, horizontal advection becomes comparable to vertical advection.

Quantitative comparisons between vertical profiles of T, T_z and w at the center of the subtropical gyre, $(x, y) = (0.5, 0.5)$ from the numerical solutions in Figure 11 with $\kappa_v \leq 0.01$, $\kappa_h = 0.002$ and from corresponding solutions of the similarity equation (6.1) are shown in Figure 19. It should be emphasized that the only free parameters in this comparison are the upper boundary conditions on vertical velocity and the upper and lower boundary conditions on temperature (and the (x, y) location; see below). Since vertical diffusion becomes significant only near the zero-crossing in the vertical velocity, and since the similarity solution has uniform temperature above the internal boundary layer, it is natural to imagine matching the diffusive solutions asymptotically to the thermostad at the base of the ventilated thermocline, rather than extending them to the surface. Accordingly, for these comparisons, the boundary conditions at $z = 1$ on temperature and vertical velocity for (6.1) were adjusted so that the solutions matched the temperature and vertical velocity at the local minimum in T_z that lies above the internal thermocline in the numerical solutions (approximately $z = 0.95$), rather than fixed to the surface temperature and the vertical velocity at the base of the Ekman layer. The temperature of the thermostad is roughly 25 units (~3°C) colder than the local surface temperature $T_E \sim T_s$, and 15 units warmer than the scaling estimate $\Delta T_i = \Delta T_{SP}$. The bottom boundary conditions were no-normal-flow ($w = 0$) and fixed temperature at $z = 0$. In the isothermal abyss, the solution for w is essentially proportional to z, so that both sides of (6.1) vanish identically. The solutions of (6.1) are not sensitive to the depth at which the bottom boundary conditions are applied, as long as it is deep enough (Stommel and Webster, 1962; Young and Ierley, 1986).

The solutions of (6.1) apparently describe well the internal thermocline in the center of the subtropical gyre (Fig. 19). However, the interior abyssal upwelling is nearly independent of longitude x in the present numerical solutions (Fig. 10), while the maximum upwelling in the Stommel-Webster solution is proportional to $(1 - x)^{-1/3}$. In this regard, the numerical solutions resemble more the solutions of the Salmon similarity equation (6.2), which have w independent of longitude. The subtropical abyssal upwelling in the numerical solutions is also only weakly dependent on latitude (Fig. 10). To the extent that the diffusively-driven upwelling in the internal boundary layer depends on the upper boundary condition on temperature, the uniformity of the subtropical abyssal upwelling is due in part to the existence of the shallow thermostad above the internal thermocline, which effectively provides a horizontally homogeneous boundary condition on temperature at the top of the internal boundary layer. The structure of this thermostad is controlled primarily by the wind-driven circulation above the internal thermocline. Thus, the ventilated circulation exerts a weak control on the diffusively-driven deep circulation in this relatively direct manner.

A generalization of the above heuristic 'asymptotic' matching might in principle allow an internal boundary layer thermocline to be consistently patched on to the base of an

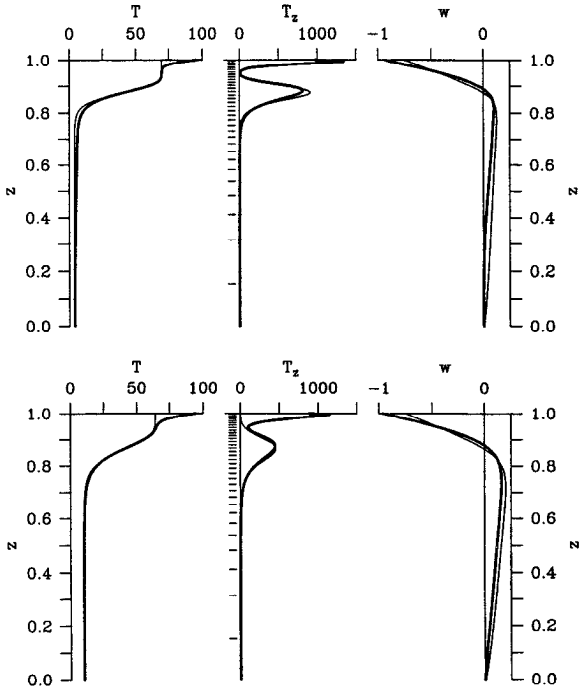

Figure 19. Vertical profiles of T, T_z, and w at $(x, y) = (0.5, 0.5)$ from the solutions in Figure 11 (thick lines) with $\kappa_v = 0.003$ (upper panels) and $\kappa_v = 0.008$ (lower panels). Corresponding solutions of the Stommel-Webster similarity equation (6.1) are also shown (thin lines).

adiabatic ventilated thermocline, in order to obtain a small-diffusion perturbation theory for the diffusively-driven meridional overturning circulation and the diffusive correction to, or constraints on, an adiabatic model of the wind-driven subtropical gyre. For example, if y-derivatives may be neglected near the center of the subtropical gyre, a local internal boundary layer approximation might be developed in which slow spatial variations in isotherm slope allow the term M_xM_{zzz} in (2.17) to be approximated locally by a constant times M_zM_{zzz}. This should yield a local version of the equation ultimately solved by Young and Ierley (1986) in their asymptotic analysis of (6.1), without the similarity restriction on the zonal structure.

Even in the absence of a fully self-consistent matched asymptotic theory, the heuristic matching of the similarity solutions illustrates the manner in which the internal thermocline in the model numerical solutions is governed by the advective-diffusive dynamics of an internal boundary layer. A related perturbation theory for the interaction of the wind-driven circulation with thermal processes, which depends on the specification of global net air-sea buoyancy fluxes as a function of density class, has been developed by Tziperman (1986). The present calculations suggest that in the small-diffusion, closed-basin limit, the subtropical abyssal stratification collapses to a thin internal boundary layer, through which

the net buoyancy fluxes in density classes might instead be deduced as a result of the asymptotic theory.

b. Diapycnal fluxes and the deep meridional cell. The original object of the Stommel and Webster (1962) calculation was to obtain a theoretical estimate of the magnitude of the abyssal upwelling velocity of the thermohaline meridional overturning calculation. The preceding comparison illustrates that at the center of our domain (at $(x, y) = (0.5, 0.5)$), such a calculation does provide a useful estimate of T_z and w in the internal thermocline in the numerical solutions, and of the dependence of these quantities on the vertical diffusivity κ_v. Evidently, the central subtropical gyre contribution to the diffusively-driven meridional overturning cell in the numerical solutions is controlled to first order by the vertical diffusivity according to the physical balances represented in the similarity solutions.

This picture of the diffusively-driven deep meridional cell appears to be independent of both the momentum balance and the heat balance in the western boundary current (at least to the extent that the temperature difference across the internal thermocline may be approximated by ΔT_{SP}, rather than being determined empirically from the numerical solutions as in Fig. 19). However, the southward meridional flow that closes the overturning cell occurs in a western boundary current (Fig. 3). In addition, most of the internal thermocline is a recirculation regime (Fig. 6). That is, fluid parcels in the internal thermocline pass through the western boundary current and return to the interior without experiencing the direct influence of air-sea interaction and the associated strong diapycnal mixing. Thus, it might be expected that the western boundary current dynamics and thermodynamics play a controlling role in this circulation.

We have argued above that the net diffusive fluxes across isopycnals are controlled by vertical diffusion in the basin interior, and not by horizontal diffusion across the tilted isopycnals of the western boundary current, at least for $\kappa_h = 0.002$ (10^5 cm^2 s^{-1}). Thus, to first order, the western boundary current transports mass adiabatically. This does not mean that the western boundary current is dynamically 'passive,' but only that extensive water mass conversion in the western boundary current does not occur in these solutions. The quasi-adiabatic recirculation of interior fluid through the western boundary layer is an essential part of the circulation associated with the internal boundary layer, whose vertical structure is controlled by the weak vertical advective-diffusive balance examined in the preceding section. In contrast, horizontal diffusion may be important in these solutions in the subpolar gyre.

The boundary currents are only marginally resolved by the numerical grid. We have carried out a limited number of additional integrations in order to assess the influence of friction and of boundary layer resolution on the present solutions. Although the former is a physical parameter and the latter primarily a numerical issue, we discuss them together because they are related by the dependence of the boundary layer width on ϵ, and because we have investigated both only briefly. A solution was obtained for the same parameters as

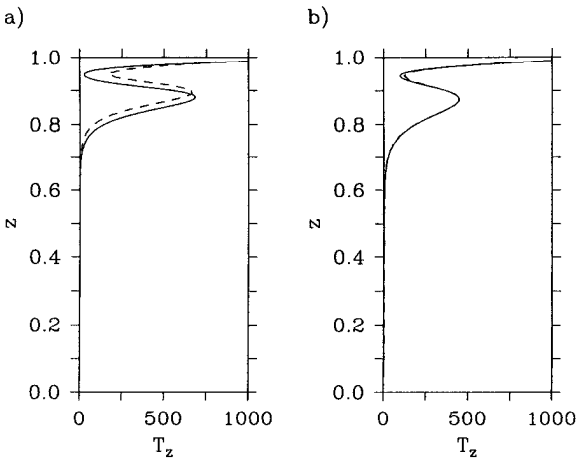

Figure 20. (a) Vertical profile of T_z at $(x, y) = (0.5, 0.5)$ with $\kappa_v = 0.004$ from the solution in Figure 11 (solid line) and a solution with $\epsilon = 0.08$ (dashed line). (b) Vertical profile of T_z at $(x, y) = (0.5, 0.5)$ with $\kappa_v = 0.008$ from the $65 \times 65 \times 64$ solution in Figure 11 (solid line) and a $33 \times 33 \times 32$ solution with a stretched zonal coordinate (dashed line).

the $\kappa_v = 0.004$ case in Figure 11 but with $\epsilon = 0.08$. The doubling of the frictional coefficient alters the interior vorticity balance. At basin center, this causes a decrease of roughly 0.02 (100 m) in the depth of the T_z maximum, but the internal thermocline (Fig. 20a) and the upwelling velocity at its base (not shown) are virtually unchanged except for this vertical translation. The central subtropical gyre contribution to the meridional overturning stream function is nearly unchanged with doubled friction, indicating that the meridional pressure gradients necessary to maintain the associated return flow adjust to carry a volume flux that is determined by the interior vertical diffusion. In contrast, the contributions from the tropical and subpolar regions do change significantly.

This comparison tests only whether the local structure of the subtropical internal thermocline is parametrically dependent on the *ad hoc* linear friction for these relatively large values of the friction coefficient ϵ. If friction were instead reduced (as would be desirable) to much smaller values, the result could be different. Jarvis and Veronis (1994) have shown that an adiabatic two-layer planetary geostrophic model exhibits a baroclinic separation of the western boundary current when the linear drag is reduced to values corresponding to $\epsilon \sim 10^{-3}$, an order of magnitude smaller than values considered here. We do not rule out the possibility that solutions of the present model with much smaller friction might differ significantly from those obtained here with $\epsilon \sim 10^{-2}$.

A second solution was obtained for the same parameters as the $\kappa_v = 0.008$ case in Figure 11 ($\epsilon = 0.04$) but using a stretched $33 \times 33 \times 32$ grid with enhanced zonal resolution near the western boundary. The smaller total number of grid points was used to reduce computational demand, which was increased substantially by the small time-steps required for the finer grid, and the intermediate κ_v case was chosen so that the interior

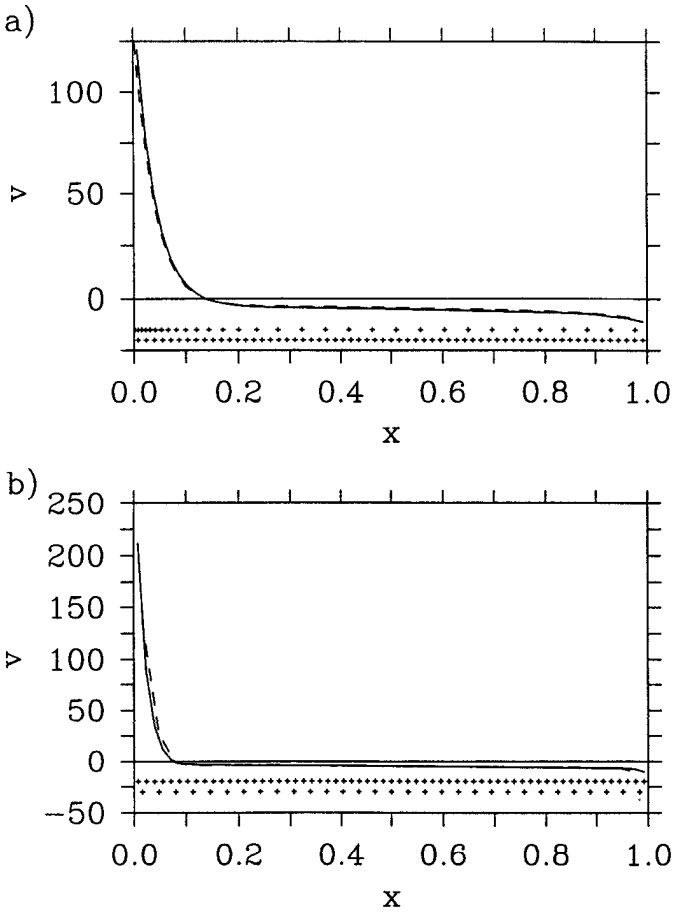

Figure 21. Zonal profiles of meridional velocity v at $(x, z) = (0.5, 0.95)$ from (a) the two solutions in Fig. 20b and (b) for the $65 \times 65 \times 32$ solution in Figure 2 (solid line) and a $33 \times 33 \times 32$ solution with the same parameters (dashed line). The zonal grids are indicated (+).

stratification would be relatively well resolved by the coarser vertical grid. The eastern boundary layer was not well resolved by the stretched grid. The solution with the stretched grid does not differ dramatically from the nominal solution. The most notable changes to the central subtropical gyre stratification are associated with the reduced vertical resolution in the shallow thermostad (Fig. 20b). The boundary layer jet is better resolved, but the improved resolution does not lead to first order changes in the velocity structure (Fig. 21a). Solutions with $\epsilon = 0.02$ on regular $33 \times 33 \times 32$ and $65 \times 65 \times 32$ grids also do not show strong dependence of the interior flow or the western boundary layer jet on resolution (Fig. 21b). Most solutions were obtained initially on 33×33 horizontal grids, interpolated to 65×65, and integrated to a final state. This proved efficient, as the 33×33 and 65×65

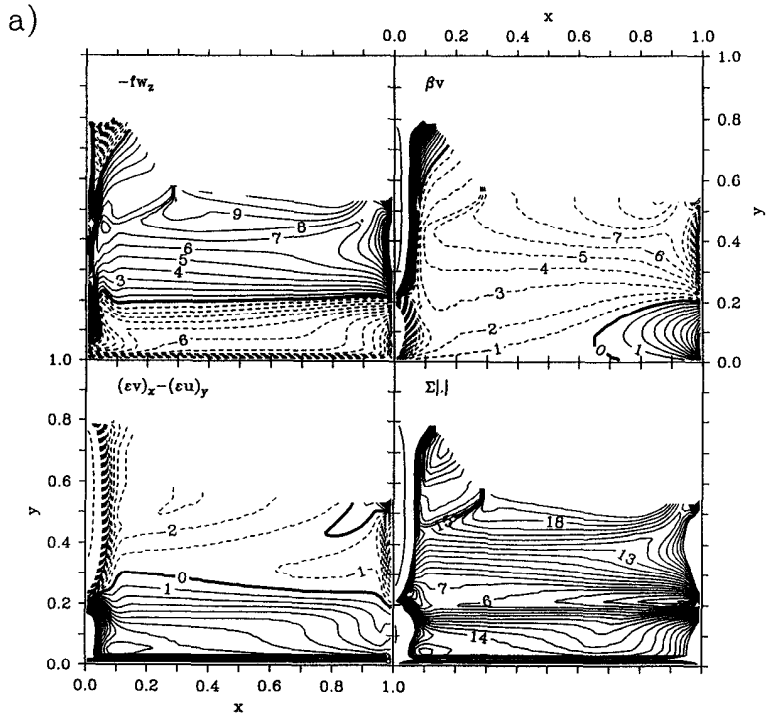

Figure 22. Vorticity balance on the isopycnal surface $T = 110$ for (a) Case 1, the solution in Figure 2, and (b) Case 2, with $\epsilon = 0.002$ in the interior. The contour interval is 1 between -20 and 20, and the -100 and 100 contours are also shown. The lower right panels show the sums of the absolute values of the three terms shown individually.

solutions did not generally differ substantially. These limited tests suggest that the present numerical solutions are probably not strongly resolution dependent.

7. Comparison with ventilated thermocline theory

a. Three-layer model. Although the circulation described above is essentially adiabatic on near-surface isopycnals, the vorticity balance is relatively viscous, with the ratio of the friction and beta terms in (2.11) reaching values as large as 0.3 in the interior (Fig. 22a). If ϵ were reduced in the interior, a better comparison could be made with the ideal fluid ventilated thermocline theory of Luyten *et al.* (1983). Holding the diffusion fixed and decreasing the friction destabilizes the solution to long baroclinic waves (Colin de Verdiere, 1986). In order to compare isopycnal slopes with the steady ventilated thermocline theory, it is thus necessary to increase the diffusion sufficiently so that the solutions remain steady for small friction. A spatially-variable friction coefficient may be introduced to replace the constant ϵ, so that the interior friction may be substantially reduced while the friction near lateral boundaries is maintained at a value that allows resolution of the lateral

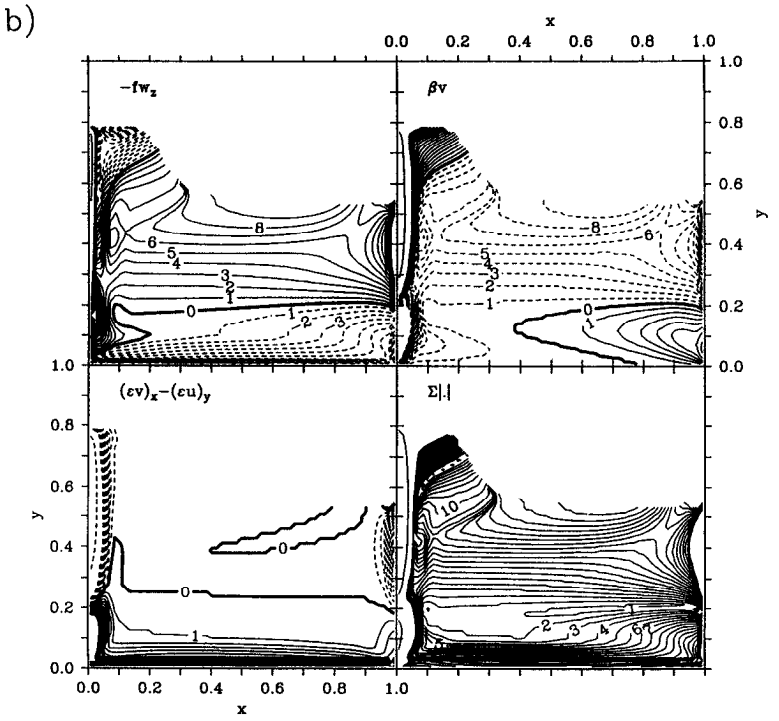

Figure 22. (Continued)

boundary layers. This changes Eq. (2.10), by introducing terms proportional to the horizontal derivatives of ϵ as in (2.13), but otherwise leaves the form of the equations unchanged. For the present comparison, a solution (Case 2) was obtained for ϵ decreasing from 0.02 on the boundary and matching quadratically to a uniform interior value of 0.002 along a contour 0.1 units inside the boundary. The diffusion coefficients were $\kappa_v = 0.008$ (0.4 cm^2 s^{-1}) and $\kappa_h = 0.08$ (4×10^6 cm^2 s^{-1}), roughly twice the values used in Case 1 above. The Case 2 solution was obtained using the alternate surface layer scheme discussed above at the end of Section 2. This is sufficient for the following comparison, to which the quantitative details of the global heat budget are not central.

Even for these larger diffusivities, the heat balance on shallow isopycnal surfaces that outcrop in the subtropical gyre is dominated by advection, although diffusion becomes important near the surface in the southwest part of the subtropical gyre. Since the interior vorticity balance is nearly inviscid (Fig. 22b), and since the rapid timescale of air-sea interaction results in an effective boundary condition of fixed temperature at the surface, the ventilated thermocline dynamics control the stratification of the upper thermocline. For simplicity, a corresponding ventilated thermocline solution was obtained for the original three-moving-layer model of Luyten *et al.* (1983). The western boundary was removed, so that no separate treatment would be required on characteristics entering the interior from

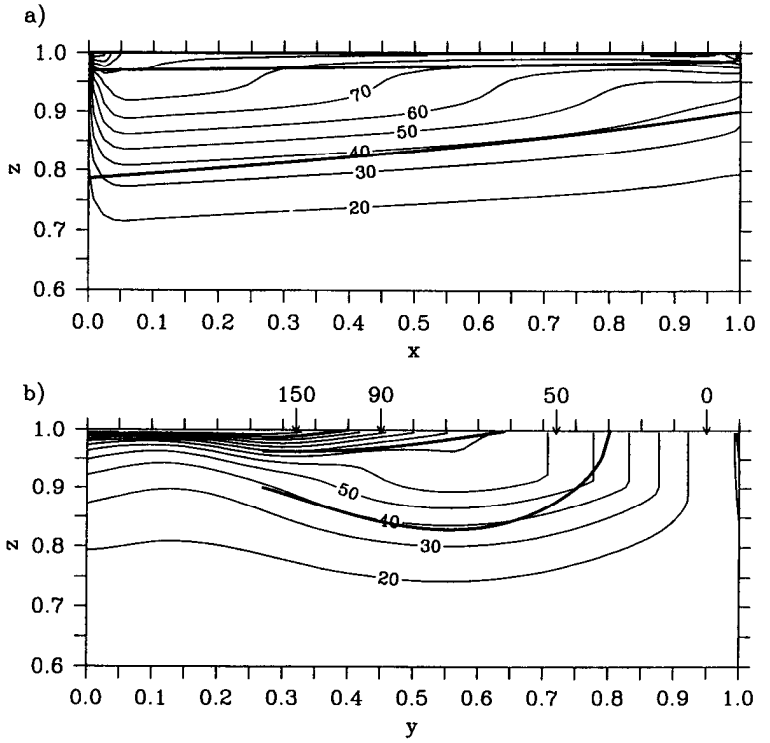

Figure 23. (a) Zonal and (b) meridional cross-sections of temperature T from Case 2, the numerical solution in Figure 22b. The layer interfaces from a three-layer ventilated thermocline solution are also shown (thick lines). The densities of the ventilated thermocline layers are indicated in (b). Only the fluid above $z = 0.6$ is shown; the deeper fluid is nearly homogeneous.

the west. All parameters were computed directly from the boundary values except the depth H_0 of the deepest moving layer (layer 3) at the eastern boundary, which was estimated from the numerical solution. In accordance with the discussion above, the density difference across the base of the deepest moving layer was taken equal to the air temperature difference across the subpolar gyre (so $\gamma_3 = 50$, in the notation of Luyten *et al.*, (1983)), while the differential densities ($\gamma_2 = 40$, $\gamma_1 = 60$) and (longitude-independent) outcrop latitudes ($y_2 = 0.65$, $y_1 = 0.45$) of the two upper layers were chosen from the air temperature distribution in the subtropical gyre. In the present case, H_0 may be defined as the mixed-layer depth at the subpolar-subtropical gyre boundary, rather than as the depth of the deepest moving layer at the eastern boundary, as in Luyten *et al.* (1983). Thus, layer 3 is to be interpreted physically as a vertically-mixed layer of 'mode water,' while layers 1 and 2 are to be interpreted as a crude representation of continuously stratified near-surface fluid.

The layer interfaces from the three-layer ventilated thermocline solution closely follow the isotherm depths from the Case 2 solution in the subtropical gyre (Fig. 23). Since the

position of the deep interface (internal thermocline) depends only weakly on the upper stratification, the degree of correspondence between the position of the deep interface and the location of the internal thermocline is primarily a measure of the dominance of the inviscid terms in the vertically-integrated vorticity balance (the Sverdrup balance) is the numerical solution. The ventilated thermocline theory describes the structure of the shallow isopycnals that outcrop in the subtropical gyre, that is, the position of the upper two interfaces in the three-layer model. These layer interfaces lie nearly parallel to the isotherm contours in the numerical solution. The deep mixed-layer (layer 3) and the motionless abyssal layer in the ventilated thermocline solution are generally 10–20 units (1–2 K) cooler than the corresponding thermostads in the numerical solution. This difference is due to the warming of the subpolar gyre by the diffusively-driven meridional overturning circulation, and to the warming of the northern subtropical gyre by advection in the western boundary current.

In the western subtropical gyre, the base of the shallow thermostad in the numerical solution is less than half as deep as the layer 3 interface (Fig. 23a). A substantial part of the Sverdrup transport in this region is carried in the temperature range 40–70, beneath the thermostad and in the recirculating part of the internal thermocline but above the maximum in T_z. The stratification and circulation in this region are influenced by horizontal diffusion in the western boundary current, due to the large horizontal diffusivity $\kappa_h = 0.08$ (4×10^6 cm^2 s^{-1}) used to obtain a steady state solution. As horizontal and vertical diffusion are reduced, and the internal thermocline collapses vertically to a discontinuity (Section 6), the Sverdrup transport in this region will apparently be carried entirely in a deep mixed layer whose outcrop extends northeastward from the southern limit of the western boundary current outflow (Section 7b).

The shadow zone of stagnant flow in layer 3 in the southeast part of the subtropical gyre that is predicted by the ideal fluid theory is relatively small, because of the relatively small layer-3 eastern boundary depth $H_0 = 0.1$ (500 m), and does not have a well-defined counterpart in the present numerical solution. In this solution, motion in the shadow zone region may also be driven by diffusion and friction, which allow flow on isopycnal surfaces across contours of potential vorticity (Fig. 9). Diffusively-driven flow in the shadow zone has been studied by Pedlosky (1987a) and de Szoeke (1995). As the wind forcing is increased, and the internal thermocline deepens, a more recognizable shadow zone appears in the numerical solutions.

Consideration of the subtropical gyre heat balance of the ventilated thermocline in the limit of small diffusion appears to lead to a paradox (Salmon, 1990). In that limit, the heat flux through the thermocline at the base of the wind-driven motion vanishes, since the vertical velocity and the diffusive heat flux $F_H \sim \kappa \Delta T_i / \delta_i \sim \kappa^{1/2}$ both vanish. Thus, a closed heat balance must exist within the wind-driven fluid layer. Persistent Ekman downwelling of warm subtropical surface water might then be anticipated to result in vertical and horizontal homogenization of temperature in the wind-driven layer. The circulation avoids this fate in the present model primarily by releasing heat (which has been gained at the

surface in the tropics) to the atmosphere in the northwest part of the gyre, where cooling of the surface layer and convective adjustment allow air-sea fluxes to penetrate to depths of several hundred meters and remove heat directly from subsurface fluid. Note also that the form of the thermal forcing used by Salmon (1990; Eq. (6.18)) favors homogenization, since the heat flux vanishes when the average gyre surface temperature reaches a specific value, after which the recirculating subtropical gyre fluid can homogenize without inducing any local heating.

b. Subtropical 'mode water'. A striking feature of the present numerical solutions is the shallow thermostad in the subtropical gyre between the upper ventilated thermocline and the internal thermocline. Two distinct mechanisms contribute to the formation of this 'subtropical mode water.'

One of these mechanisms operates at the subtropical-subpolar gyre boundary. For small diffusion, the internal boundary layer resembles a material surface that separates warm subtropical fluid from cold abyssal fluid, and a natural correspondence with two-layer planetary geostrophic ocean models (Parsons, 1969; Veronis, 1973) emerges (Salmon, 1990). In order that the volume of warm fluid remain constant in the two-layer model, the southward Ekman transport across the subtropical-subpolar gyre boundary must be balanced by an equal northward geostrophic transport, and this in turn requires that the interface be depressed at the eastern boundary (Parsons, 1969; Veronis, 1973). In the present model, this balance leads immediately to the formation of a thermostad along the gyre boundary. At the gyre boundary, the air temperature ΔT_{SP} (see Fig. 1) determines the temperature of the surface fluid away from boundary currents (Section 4). Since this is the coldest fluid entering the subtropical gyre, the warmest (uppermost) fluid in the internal thermocline must have this same temperature ΔT_{SP}. Consequently, the fluid between the surface and the top of the depressed internal thermocline must have uniform temperature ΔT_{SP}, and an 'eastern' mode water layer must form at the gyre boundary.

The thickness of this mode water at the gyre boundary may be identified with the fixed eastern boundary depth H_0 of the deepest ventilated layer in the three-layer calculation of the preceding section. Since the transport balance determines only the difference in interface depth from east to west (Parsons, 1969; Veronis, 1973), it does not determine H_0. In the numerical solutions, however, the isopycnals of the internal thermocline are typically close to and beneath the surface along the western boundary at the latitude of the gyre boundary. In this case, the depth H_0 may be estimated directly from the transport balance to show the explicit dependence on the wind stress,

$$H_0 = (2\tau_M/\Delta T_{SP})^{1/2} \sim (w_{E0}/(\pi \Delta T_{SP}))^{1/2}. \tag{7.1}$$

Here τ_M is the zonal component of the wind stress (assumed independent of x) at the gyre boundary, where the curl of the wind stress vanishes (slightly north of the point where $w_E = 0$). If an estimate of H_0 is obtained from the present calculations by computing the

maximum mixed-layer depth along the subtropical-subpolar gyre boundary, this depth correlates roughly with the expression (7.1) for a wide range of values of w_{E0} (Fig. 12).

The situation that arises at the gyre boundary is thus similar to that envisioned by Pedlosky (1987b), who argued that (7.1) should be a lower bound on the thickness of the active layer. In the present case, this lower bound appears also to be an approximate upper bound, as excess warm fluid tends to be expelled from the subtropical gyre as the steady state is approached, perhaps because warm fluid flowing down the mean pressure gradient and into the subpolar gyre can cool by contact with the atmosphere. The surface warming required to balance the southward Ekman transport of cold fluid across isopycnal outcrops in the boundary current outflow (Nurser and Williams, 1990) is supported by northward baroclinic geostrophic heat transport in the boundary current, which cannot be represented in the two-layer model, and not by air-sea exchange. Although the present model does include thermodynamic processes that are neglected in the two-layer model, it also has a strongly frictional downstream momentum balance, which may inhibit any tendency toward separation of the boundary current (Jarvis and Veronis, 1994). If such separation were to occur with smaller friction in the present model, the estimate (7.1) would be inaccurate. In our solutions, separation does not occur, and H_0 may be estimated from (7.1), which effectively completes a first-order closure of the three-layer ventilated thermocline calculation presented above.

With H_0 given, the ventilated thermocline dynamics determine the solution along characteristics (trajectories) that leave the surface layer in the subtropical gyre or the deep mixed layer adjacent to the gyre boundary. A third class of trajectories enters the subtropical gyre interior from a deep surface mixed layer that forms adjacent to the western boundary current. The mechanism that generates the western deep mixed layer is different from that operating at the gyre boundary, and is most easily understood in terms of the flow on isopycnal surfaces, such as those shown in Figure 6a and Figure 9. Along the eastern part of the outcrop line, these surfaces are ventilated from the subtropical surface layer by Ekman pumping, essentially as envisioned by Luyten *et al.* (1983). To the west, flow exits the isopycnal surface as it cools by vertical diffusion and convective adjustment in the western boundary current outflow. The western mode water layer, which is marked by the tightly packed depth contours in Figure 6a and the potential vorticity minimum in Figure 9a, forms on each isopycnal surface at the point along the outcrop where the flow across the outcrop vanishes. Southwest of this point, the flow on the isopycnal surface recirculates through the western boundary current without being exposed to air-sea exchange processes.

The fluid in the recirculation region is set in motion only by diffusion, and forms part of the internal thermocline. In the limit of small diffusion, there is no source of fluid or motion in this region, and the recirculation collapses vertically into a discontinuity along with the rest of the internal thermocline. In the terminology of the ventilated thermocline (e.g., Huang, (1991), Fig. 2), this collapsed recirculation may be said to inhabit the western 'pool' region defined by upper layer characteristics that leave the western boundary.

Consequent to this collapse, the surface mixed layer that forms at the boundary of this region must itself extend downward to the internal thermocline, since it lies immediately above a recirculation region on the next denser isopycnal surface, which in turn must collapse with the internal thermocline. On each isopycnal surface, the western 'mode water' layer forms as this mixed layer subducts. In other words, the thermostad forms because of an absence of sources of fluid on recirculating trajectories on the denser isopycnal surface at its base. The set of mixed layer subduction points, which correspond to the southernmost points of the deep surface mixed layers and to the points at which the velocity on each isopycnal outcrop is tangent to the outcrop line, form a line that tends northeastward from the southernmost point of western boundary current outflow, toward the subpolar gyre boundary (Fig. 6, Fig. 8), whose orientation will be influenced by the local timescale of air-sea exchange. The mixed-layer density along this contour is determined by the local air temperature, since each point is located precisely where the sign of the air-sea heat exchange changes as the isopycnal outcrop is traversed. The depth of the mixed layer at each of these subduction points, and thus the thickness of the western mode water, is determined recursively westward by the Sverdrup balance at the contour, with the depth of the isopycnals to the east set by the ventilated thermocline dynamics, the eastern boundary condition H_0 for the depth of the moving fluid, and the subduction of the mixed layer at the previous point to the northeast along this contour.

These arguments suggest that the structure of the shallow thermostad in the model is controlled by large-scale dynamic and thermodynamic processes. The proximate, local cause of the model thermostads is convective adjustment, primarily in association with surface cooling. The accuracy of this parameterization is unknown. In addition, it should be noted that the use of such a scheme interrupts the correspondence between the differential equations and the numerical result, as the solution in the convecting regions is comprised of a time-step using (2.1)–(2.5) followed by a discrete adjustment of the density field that is constrained only by the requirements to prevent static instability and conserve heat in columns. This temporally discrete adjustment is likely to have different convergence properties than the discretization of the evolution equations, and disturbs the smoothness of the solution at the edges of the convective regions. Although we suspect that this difficulty is not severe, it deserves future attention.

8. Western boundary current

In the present model, the western boundary current is supported by a simple *ad hoc* representation of frictional and diffusive processes (Samelson and Vallis, 1997). This distinguishes it from the interior flow regimes, which are supported to a greater degree by dynamic balances that result from deductive scale-asymptotic simplifications of the fluid and thermodynamic equations. Thus, the details of the flow in the western boundary regime are of physical interest only to the degree to which they influence the interior flow, and accordingly have been discussed where appropriate in the preceding analysis of the interior flow regimes. For reference, we briefly summarize the boundary current heat and vorticity

balances here. To first order, the vorticity balance (2.11) is $\beta v \sim -\epsilon v_x$ (Fig. 22), resulting in an approximately exponential meridional jet with e-folding thickness ϵ/β and maximum velocity at the boundary (Fig. 21). The condition that normal heat flux vanish at the boundary is met by the balance (2.13) of opposing Fickian and higher-order diffusive fluxes, and the choice (2.16) for the biharmonic diffusivity extends this balance, to first order, through the ϵ/β boundary layer. In combination with a small horizontal diffusivity, this results in a western boundary current that is sufficiently adiabatic that the net diffusive fluxes across isopycnal surfaces are not dominated by horizontal diffusion across the sloping isotherms of the western boundary current (Fig. 14a, Fig. 18). The no normal flow condition requires a balance between the alongshore pressure gradient and the frictional drag on the alongshore flow, so an alongshore pressure gradient must develop to support the nearly geostrophic western boundary current. Integration of this boundary condition around the boundary shows that the net circulation at the boundary must vanish at each interior level. This illustrates that the boundary current can in principle exert an important controlling influence on the interior flow, as argued for a similar model by Winton (1996). It seems likely that a complete understanding of the meridional overturning circulation in the present model would require a thorough analysis of the boundary currents and their interaction with the inferior flow.

9. Comparison with observations

Although the forcing fields and basin geometry for the solutions discussed above are highly idealized representations, it is useful to briefly compare the qualitative features of the solutions with oceanographic observations. For the values given in Section 4, with $\Delta T_a = 2\Delta T_i = 20\text{K}$, the ratio $\delta_i/D_a = 0.25 - 0.75$ for $\kappa = 0.1 - 1\ \text{cm}^2\ \text{s}^{-1}$. Thus, the scaling estimates suggest that the two thermocline regimes should be distinguishable in the ocean, with the internal thermocline forming a thick internal boundary layer at the base of the ventilated thermocline in the subtropical gyre.

If the model results are compared to hydrographic observations of the North Atlantic, a striking difference is found between the model and observed abyssal stratification. Profiles of buoyancy frequency from the model and the North Atlantic have some general similarities in and above the main thermocline, but at greater depth the model buoyancy frequency is much smaller than the observed buoyancy frequency (Fig. 24). Some of the quantitative agreement in the main thermocline is due to the smaller total density difference between the surface and the abyss in the model than in the observations. A larger air temperature gradient in the model leads to a larger density difference across the internal thermocline, but no significant strengthening of the abyssal stratification. Larger diffusivities lead to a broader, weaker and deeper internal peak in buoyancy frequency, but in general do not substantially improve qualitative agreement with the more uniform observed abyssal stratification, while degrading the agreement with the observed internal peak. A similar weak abyssal stratification has been found previously in primitive equation

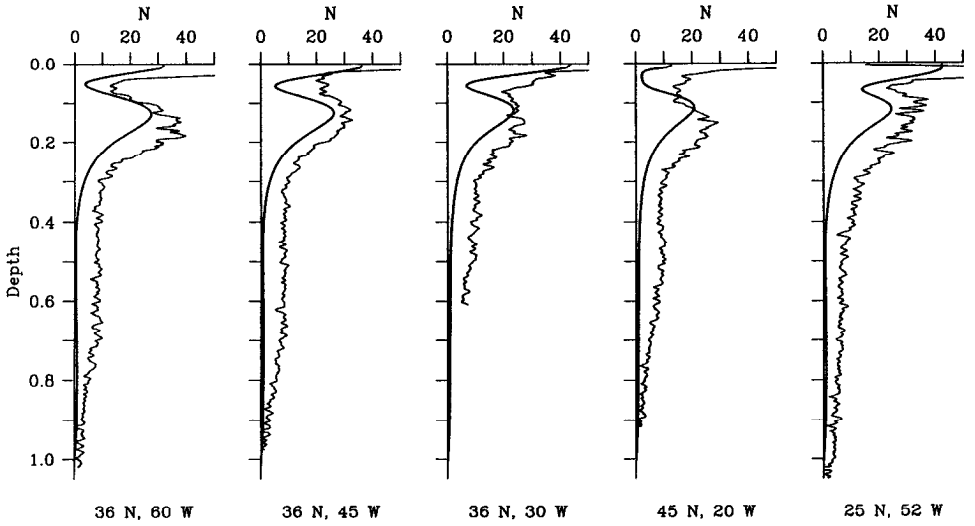

Figure 24. Nondimensional observed (thin line) and model (thick line) buoyancy frequency versus depth at five locations in the subtropical gyre. The observed profiles are from the 36N section in Figure 25a, at 60W (left panel), 45W (center left), and 30W (center right), from a station at 45N, 20W from the cruise described by Tsuchiya *et al.* (1992), and from 25N, 52W from the section in Figure 25b. The model profiles are from the solution in Figure 11 with $\kappa_v = 0.004$, at $x = [0.25, 0.5, 0.75]$, $y = 0.5$, at $(x, y) = (0.83, 0.74)$, and at $(x, y) = (0.38, 0.38)$. Buoyancy frequency is scaled by 0.075 cph and depth by 500 km.

general circulation models (Cummins, 1991). Evidently, fundamental aspects of the physics of the deep circulation are missing from, or misrepresented in, the present model.

In and above the internal thermocline, some resemblance of zonal and meridional cross-sections of T $(-\rho)$ from the numerical solutions (Fig. 5) to corresponding cross-sections of σ_θ from the North Atlantic (Fig. 25) may be noted. In the subtropical gyre, there is an internal maximum (the 'main thermocline') in the stratification near 750 m depth, and a secondary maximum near the surface (Fig. 25). The two maxima join toward the southern edge of the subtropical gyre, and there is a sharp pycnocline in the tropics, which weakens rapidly with depth, and the main thermocline rises toward the surface as the subpolar gyre is approached. A double-thermocline structure is most apparent in the western subtropical gyre, where the 18-degree water forms a thick thermostad above 500 m depth, but there is some indication of a shallow minimum in the stratification near 350 m that extends eastward across the basin even at 36N (Fig. 25b). The eastern minimum is more evident in the latitude band 40-50 N (McCartney and Talley, 1982, their Figure 11).

The 18-degree thermostad and the shallow eastern minimum in stratification are signatures of convectively formed subtropical mode waters (McCartney, 1982; McCartney and Talley, 1982; Tsuchiya *et al.*, 1992). The shallow thermostad above the internal thermocline in the numerical solutions may be an idealized analog of these observed mode waters. However, there are significant differences between the spatial distributions of the

model and observed mode waters. The 18-degree subtropical mode water is concentrated in the northwestern part of the North Atlantic. A colder variety is found in the northeast part of the gyre, with only a mild weakening of the shallow pycnocline at intermediate longitudes. The structure of the model thermostad is more nearly uniform across the basin. Nonetheless, two distinct sets of dynamic and thermodynamic processes control the formation of the thermostad in the model, one at the western boundary current outflow and a second along the gyre boundary. If an identification of model and observed mode waters were to be made, the present results would suggest that the 18-degree mode water may form in part because of an effective absence of sources of fluid on recirculating trajectories on the denser isopycnal surfaces at the base of the thermostad, while the eastern subtropical-subpolar mode waters may form as a consequence of cross-gyre transport and thermodynamic balances, and the weakness of diapycnal motion in the subtropical main thermocline. Previous theories of 18-degree water formation (Dewar, 1986; Cushman-Roisin, 1987) have focused on the roles of diffusion and surface cooling in maintaining weakly-stratified recirculating fluid in quasi-geostrophic approximation. The present results suggest that the thickness of the mode water layers may also be related to the large-scale wind forcing.

10. Summary

We find that, in a simple closed-basin planetary-geostrophic model of the large-scale circulation, two distinct thermocline regimes occur simultaneously provided the diapycnal diffusion is sufficiently small (Fig. 1). On isopycnal surfaces that outcrop in the subtropical gyre, surface thermal forcing, Ekman downwelling, advective dynamics, and convective adjustment combine to produce a shallow thermocline regime whose essential dynamics are described by the ideal fluid ventilated thermocline theory of Luyten *et al.* (1983). The deepest ventilated fluid is a weakly stratified layer ('mode water') that forms by different mechanisms at the subtropical-subpolar gyre boundary and along the western boundary current outflow. The depth of this layer at the gyre boundary may be estimated from a formula of Pedlosky (1987); this appears to close the ventilated thermocline theory of the wind-driven motion in the adiabatic limit, since it provides an eastern boundary condition for the deepest ventilated layer. At the base of the ventilated thermocline, near the zero-crossing of the vertical velocity, vertically convergent thermal advection from Ekman pumping above and thermally-driven abyssal upwelling below balance vertical thermal diffusion to produce an internal thermocline whose essential dynamics are described by the internal boundary layer theory of Stommel and Webster (1962). The numerical solutions compare quantitatively as well as qualitatively with the ventilated thermocline and internal boundary layer theories. The horizontal circulation in the abyssal thermostad is controlled by diffusively-driven upwelling at the base of the internal boundary layer, as in the abyssal circulation theory of Stommel and Arons (1960).

The temperature difference across the ventilated thermocline is directly related to the meridional surface temperature difference across the subtropical gyre. The temperature of

a)

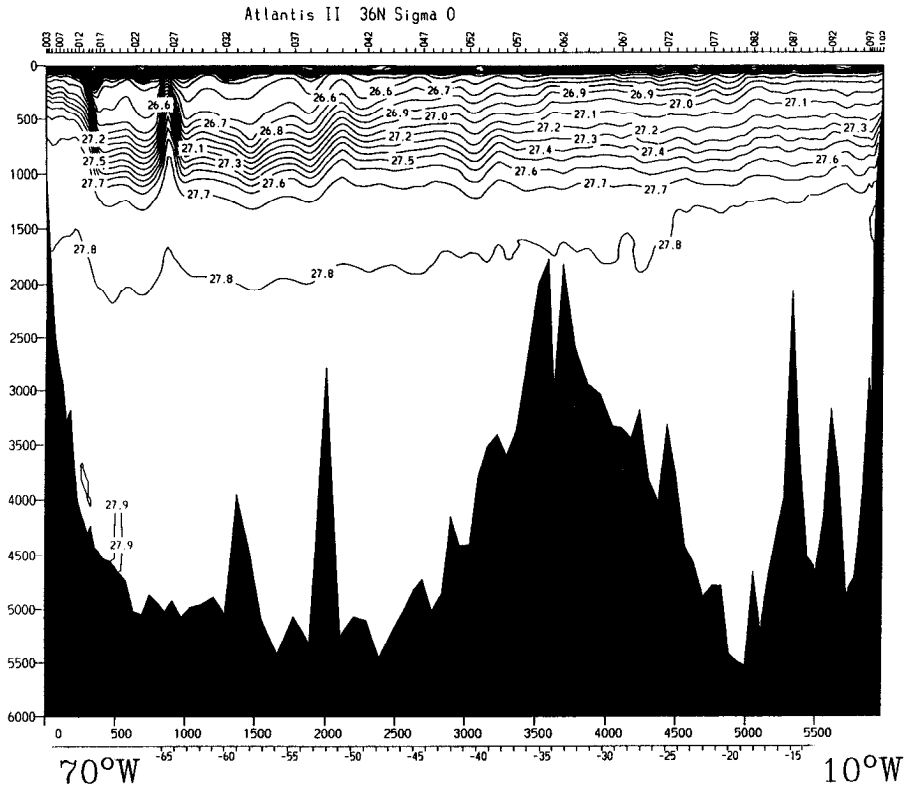

Figure 25. (a) Zonal (36N) and (b) meridional (53W) cross-sections of σ_θ from the North Atlantic. Note that σ_θ is not an accurate measure of abyssal stability. (Courtesy of L. Talley.)

the deepest ventilated fluid is roughly equal to the surface temperature at the northern edge of the subtropical gyre (the latitude where the Ekman downwelling vanishes), and since this is essentially the same as the surface temperature at the southern edge of the subpolar gyre, the temperature difference across the internal thermocline is directly related to the temperature difference across the subpolar gyre, and not to the basin-wide meridional temperature difference. Thus, in the limit of small diapycnal diffusion, the ventilated thermocline effectively insulates the unventilated interior from surface conditions in the subtropical gyre, and the strength of the meridional overturning circulation depends to first order only on the surface temperatures in the subpolar gyre. Warmer subtropical gyre surface temperatures reach the top of the internal thermocline toward the center of circulation of the subtropical gyre, where the western variety of subtropical mode water forms in the western boundary current outflow.

The quantitative correspondence between the numerical solutions and the ventilated and internal boundary layer thermocline theories is sufficiently close, and the thermocline

b)

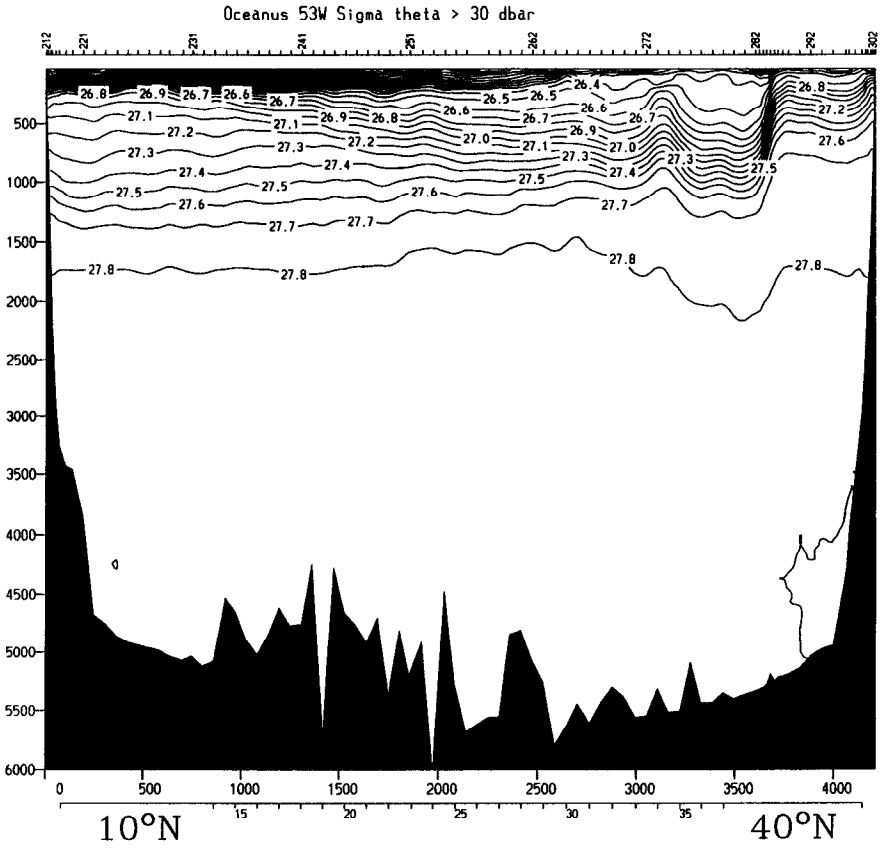

Figure 25. (Continued)

components described by the theories sufficiently simple and regular, that the interior structure of the closed-basin numerical solutions may be approximated to first order by the limited-domain theoretical models, using simple rules to relate the surface boundary conditions to appropriate 'interior' boundary conditions for the theoretical models. In the small diffusion limit, the entire subtropical gyre above the internal thermocline is evidently ventilated by trajectories that enter the interior either from the surface Ekman layer or from a deep mixed layer that forms along the western boundary current outflow and the subtropical-subpolar gyre boundary, and the diffusively-driven abyssal circulation vanishes as the internal thermocline collapses to a discontinuity at the base of the ventilated thermocline. In this limit, then, the deep 'unventilated' recirculation regime of the Rhines-Young theory disappears, and the Sverdrup transport is distributed between the surface and the internal thermocline.

The numerical calculations crudely resemble the observed stratification of the North

Atlantic in and above the main thermocline, that is, to a depth of 1500 m. Below the main thermocline, however, the predicted stratification is much weaker than observed, as the abyssal fluid is effectively uniform. The abyssal homogenization occurs because in the absence of diffusion there is no mechanism to force heat downward from the base of the ventilated thermocline into the abyss, and consequently the abyss fills with the coldest fluid in the basin, pushing any extant warmer fluid upward. Although the present calculations were performed in a square single-hemisphere basin, there is little reason to believe that the abyss would not homogenize in a similar manner in more complex simply-connected geometries with spatially complex (but steady) forcing fields (e.g., Samelson and Vallis, 1996, their Figure 3). In the steady state, the rate of deep sinking of cold water is fixed to the weak diffusive heating of upwelling water, and it does not seem proper to conceive of the abyssal circulation as being driven solely or independently by cold sinking, nor to anticipate the presence of multiple sources of cold sinking fluid layering the abyss at different temperatures, since in the limit of small diapycnal diffusion only the very coldest fluid can survive beneath the ventilated thermocline.

The discrepancy between the dynamical homogenization of the abyss for small diapycnal diffusion and the observed abyssal stratification has numerous possible causes. The equator-ward flow of dense water in the abyssal ocean is likely restrained by interactions with topographic constrictions (Price and Baringer, 1994) and by the zonally-contiguous geostrophic pressure gradient of the Antarctic Circumpolar Current (Gill and Bryan, 1971; Cox, 1989; Warren, 1990; Toggweiler and Samuels, 1995). Diapycnal mixing in the abyssal ocean may occur primarily in boundary layers, perhaps in specific geographic locations (Munk, 1966; Armi, 1978; Garrett, 1991; Mudge and Lueck, 1995; Toole *et al.,* 1997); such mixing is effectively neglected in the present calculations by the use of a small uniform diffusivity. Horizontal eddy fluxes may limit the penetration of deep convection (Visbeck *et al.,* 1996), interior abyssal diffusivities may be larger than assumed here (Cummins *et al.,* 1990; Cummins, 1991), and the assumption of steady-state abyssal circulation may be inappropriate. The recent observational synthesis by Schmitz (1995) illustrates the complexity of intergyre flow in and beneath the thermocline in the global ocean.

The steady numerical solutions presented here have a complex spatial structure with a variety of flow regimes, including both horizontal and vertical boundary layers. We have focused our analysis on a central element of the solutions, the subtropical thermocline. The results appear to be consistent with some aspects of the observed structure of the ocean. However, we have not achieved a complete understanding of these solutions, let alone understood the behavior of the model for more general forcing and geometry. For example, the meridional overturning circulation in the present solutions, which appears to be strongly dependent on processes in the Ekman upwelling regions external to the subtropical gyre, remains poorly understood. Important technical issues, such as the effect of the still relatively coarse horizontal and vertical resolution of the numerical grid, and the

interplay between the convective adjustment scheme and the time-stepping solution of the partial differential equation (2.17), also remain unresolved.

Acknowledgments. We are grateful to R. Salmon, X. Huang, J. Pedlosky, R. de Szoeke, R. Williams, R. Schmitt, A. Gargett, W. Dewar, and K. Speer for conversations and suggestions, to M. Mundt for showing us how to obtain the numerical solution of the similarity equations (6.1) and (6.2), to L. Talley for providing the contoured North Atlantic σ_θ sections, and to T. McKee, B. Arbic, and B. Owens for supplying data and software for, and assistance with, the computation of buoyancy frequency profiles. R. Salmon brought the Stommel-Webster equation (6.1) to our attention following an early presentation of this work by RMS at Woods Hole. The manuscript benefited from thoughtful comments from G. Veronis and two anonymous reviewers. This research was supported for RMS by the National Science Foundation (NSF, Grants OCE91-14977 and OCE94-15512), the Office of Naval Research (Grant N00014-92-J-1589), and the Woods Hole Oceanographic Institution, and for GKV by NSF (Grants ATM 93-17485 and OCE94-15512) and UCSC. WHOI contribution number 9116.

APPENDIX

Numerical implementation

Planetary geostrophic model. Finite differencing of the planetary geostrophic model is relatively straightforward. Advection is effected using centered differencing in flux form, except at the upper boundary where an upwind scheme is implemented. Time-stepping uses a second order Runge-Kutta type algorithm.

Let the domain be covered by a three-dimensional grid, $\{i, j, k\}$ denoting increments in the x-, y-, and z-directions respectively, and let temperature, T, density, ρ, and pressure, p, be defined on that grid. Let Δx, Δy and Δz be the respective grid increments. If $i_{\max}$ and $j_{\max}$ are the number of grid points in the x and y directions, the lateral boundaries are considered to lie at $\{i = 1 + 1/2, i_{\max} - 1/2\}$ and $\{j = 1 + 1/2, j_{\max} - 1/2\}$, namely one half a grid interval in from the edge.

Define the following variables:

$$\hat{T}_{i-1/2,j,k} = \tfrac{1}{2}(T_{i,j,k} + T_{i-1,j,k}) \tag{A.1}$$

$$\tilde{T}_{i,j-1/2,k} = \tfrac{1}{2}(T_{i,j,k} + T_{i,j-1,k}) \tag{A.2}$$

$$\overline{T}_{i,j,k-1/2} = \tfrac{1}{2}(T_{i,j,k} + T_{i,j,k-1}) \tag{A.3}$$

and similarity for p and ρ.

Define also the difference operators:

$$\delta_x \phi_{i,j,k} = (\phi_{i+1/2,j,k} - \phi_{i-1/2,j,k})/\Delta x, \tag{A.4}$$

$$\delta_y \phi_{i,j,k} = (\phi_{i,j+1/2,k} - \phi_{i,j-1/2,k})/\Delta y, \tag{A.5}$$

where $\phi_{i,j,k}$ is an arbitrary field.

Then the horizontal velocities are defined on a staggered grid, obtained from pressure on as follows:

$$u_{i-1/2,j,k} = -\gamma_j(\epsilon(\, p_{i,j,k} - p_{i-1,j,k})/\Delta x + f_j(\, \hat{p}_{i-1/2,j+1,k} - \hat{p}_{i-1/2,j-1,k})/2\Delta y) \tag{A.6}$$

and

$$v_{i,j-1/2,k} = \gamma_{j-1/2}(f_{j-1/2,k}(\tilde{p}_{i+1,j-1/2,k} - \tilde{p}_{i-1,j-1/2,k})/2\Delta x - \epsilon(p_{i,j,k} - p_{i,j-1,k})/\Delta y) \tag{A.7}$$

where $\gamma_j = f_j^2 + \epsilon^2$, with f_j the Coriolis parameter.

The vertical velocity is staggered between the horizontal velocity levels. It is obtained by integrating the mass conservation equation,

$$(w_{i,j,k+1/2} - w_{i,j,k-1/2})/\Delta z = \delta_x u_{i,j,k} + \delta_y v_{i,j,k}, \tag{A.8}$$

with the vertical velocity set equal to zero at the lower boundary. The vertical grid need not be uniform, and a stretched grid is in fact normally used to give enhanced resolution in the thermocline. The vertical grid interval Δz is then in general a function of the index k.

The finite difference form of the barotropic elliptic equation (2.23) is obtained by substituting (A-6) and (A-7) into the mass conservation equation, and summing over vertical levels. The form of resulting difference equation is not particularly informative. The boundary conditions on this elliptic equation are no-normal flow, to be applied on the boundary columns and rows where u and v are respectively defined, namely $i = 1 + 1/2$ and $i = i_{\max} - 1/2$, and $j = 1 + 1/2$ and $j = j_{\max} - 1/2$. The difference form of (2.29) leads to a cyclic tridiagonal problem for the boundary values of p, with the interior values of the pressure appearing as 'forcing' terms on the right hand side, which can be rapidly solved. The elliptic problem is solved by successive over relaxation (SOR); multigrid methods would also be appropriate if speed were a consideration. The correct boundary values are obtained by recalculating them after each internal SOR iteration until the solution converges.

The (nondimensional) hydrostatic equation is differenced as follows:

$$(\, p_{i,j,k+1} - p_{i,j,k})/\Delta z = \bar{\rho}_{i,j,k+1/2} \tag{A.9}$$

The advection of temperature or salinity uses centered differences in flux form, ensuring conservation of the L_1 norm of the advected quantity. The finite difference form of the advection term is:

$$(u_{i+1/2,j,k}\hat{T}_{i,+1/2,j,k} - u_{i-1/2,j,k}\hat{T}_{i-1/2,j,k})/\Delta x \tag{A.10}$$

$$+ (v_{i,j+1/2,k}\tilde{T}_{i,j+1/2,k} - v_{i,j-1/2,k}\tilde{T}_{i,j-1/2,k})/\Delta y \tag{A.11}$$

$$+ (w_{i,j,k+1/2}\overline{T}_{i,j,k+1/2} - w_{i,j,k-1/2}\overline{T}_{i,j,k-1/2})/\Delta z \tag{A.12}$$

The harmonic horizontal diffusion terms are obtained using a standard five-point Laplacian stencil, and the biharmonic terms are obtained by iterating this once. The boundary conditions of no-normal flow and no-normal diffusive flux at the boundary determine the boundary values, the former requiring the application of the cyclic tridiagonal solver. Vertical diffusion is also implemented in a standard way. Normally a no-heat-flux condition is applied at the bottom of the domain, whereas the temperature at the top is determined from the Ekman layer dynamics, (2.19).

The overall time-stepping procedure is as follows. Given a wind field, the barotropic pressure field is obtained by solving the difference form of (2.23). Given also an initial temperature field (and salinity field if appropriate) the density field is diagnosed from an equation of state, and the complete pressure field is then obtained by vertically integrating the hydrostatic equation (A.9). The horizontal and vertical velocities are then obtained from near-geostrophic balance, (A.6, A.7) and mass conservation (A.8). These velocities are used to advance the temperature (and salinity) fields one timestep, and the process is repeated.

Similarity equations. The similarity equations (6.1) and (6.2) were solved by Newton's method (e.g. Press *et al.,* 1992) applied in physical space, using a code initially developed by M. Mundt. The equations were differenced on a uniform grid in a standard way and the solutions were obtained to the resulting difference equations, typically using 500–1000 grid points to cover the domain.

REFERENCES

Armi, L. 1978. Some evidence for boundary mixing in the deep ocean. J. Geophys. Res., *83,* 1971–1979.

Bryan, F. 1987. Parameter sensitivity of primitive equation ocean general circulation models. J. Phys. Oceanogr., *17,* 970–985.

Bryan, K. 1969. A numerical method for the study of the circulation of the World Ocean. J. Comput. Phys. *4,* 347–376.

Colin de Verdiere, A. 1986. On mean flow instabilities within the planetary geostrophic equations. J. Phys. Oceanogr., *16,* 1981–1984.

—— 1988. Buoyancy driven planetary flows. J. Mar. Res., *46,* 215–265.

—— 1989. On the interaction of wind and buoyancy driven gyres. J. Mar. Res., *47,* 595–633.

Cox, M. 1985. An eddy-resolving model of the ventilated thermocline. J. Phys. Oceanogr., *15,* 1312–1324.

—— 1989. An idealized model of the world ocean. Part I: the global-scale water masses. J. Phys. Oceanogr., *19,* 1730–1752.

Cox, M. and K. Bryan. 1984. A numerical model of the ventilated thermocline. J. Phys. Oceanogr., *14,* 674–687.

Cummins, P. 1991. The deep water stratification of ocean general circulation models. Atmos. Ocean, *19,* 563–575.

Cummins, P., A. Gargett and G. Holloway. 1990. Sensitivity of the GFDL ocean general circulation model to a parameterization of vertical diffusivity. J. Phys. Oceanogr., *20,* 817–830.

Cushman Roisin, B. 1987. On the role of heat flux in the Gulf Stream-Sargasso Sea Subtropical gyre system. J. Phys. Oceanogr., *17,* 2189–2202.

de Szoeke, R. 1995. A model of wind- and buoyancy-driven ocean circulation. J. Phys. Oceanogr., *25,* 918–941.

Dewar, W. K. 1986. On the potential vorticity structure of weakly ventilated isopycnals: A theory of subtropical mode water maintenance. J. Phys. Oceanogr., *16,* 1204–1216.

Garrett, C. 1991. Marginal mixing theories. Atmos.-Ocean, *29,* 313–339.

Gill, A. and K. Bryan. 1971. Effects of geometry on the circulation of a three-dimensional southern hemisphere ocean model. Deep-Sea Res., *18,* 685–721.

Gregg, M. 1987. Diapycnal mixing in the thermocline: A review. J. Geophys. Res., *92,* 5249–5286.

Hall, M. and H. Bryden. 1982. Direct estimates and mechanisms of ocean heat transport. Deep-Sea Res., *29,* 339–359.

Haney, R. 1971. Surface thermal boundary condition for ocean circulation models. J. Phys. Oceanogr., *1,* 241–248.

Hood, S. and R. Williams. 1996. On frontal and ventilated models of the main thermocline. J. Mar. Res., *54,* 211–238.

Huang, R. X. 1988. On boundary value problems of the ideal-fluid thermocline. J. Phys. Oceanogr., *18,* 619–641.

—— 1991. The three-dimensional structure of wind-driven gyres: ventilation and subduction. Rev. Geophys. (Suppl.) 590–609.

Jarvis, R. and G. Veronis. 1994. Strong deep recirculations in a two-layer wind-driven ocean. J. Phys. Oceanogr., *24,* 759–776.

Ledwell, J., A. Watson and C. Law. 1993. Evidence for slow mixing across the pycnocline from an open-ocean tracer-release experiment. Nature, *364,* 701–703.

Luyten, J., J. Pedlosky and H. Stommel. 1983. The ventilated thermocline. J. Phys. Oceanogr., *13,* 292–309.

McCartney, M. 1982. The subtropical recirculation of Mode Waters. J. Mar. Res., *40* (Suppl.), 427–464.

McCartney, M. and L. Talley. 1982. The subpolar mode water of the North Atlantic Ocean. J. Phys. Oceanogr., *12,* 1169–1188.

Mudge, T. and R. Lueck. 1995. Topographically induced mixing around a shallow seamount. Nature, (submitted).

Munk, W. 1966. Abyssal recipes. Deep-Sea Res., *13,* 707–730.

Nurser, A. and R. Williams. 1990. Cooling Parson's model of the separated Gulf Stream. J. Phys. Oceanogr., *20,* 1974–1979.

Parsons, A. T. 1969. A two-layer model of Gulf Stream separation. J. Fluid Mech., *39,* 511–528.

Pedlosky, J. 1979. Geophysical Fluid Dynamics, Springer-Verlag, New York, 1st ed., 624 pp.

—— 1987a. The buoyancy- and wind-driven ventilated thermocline. J. Phys. Oceanogr., *16,* 1077–1087.

—— 1987b. On Parson's model of the ocean circulation. J. Phys. Oceanogr., *17,* 1571–1582.

Phillips, N. A., 1963. Geostrophic motion. Rev. Geophysics, *1,* 123–176.

Press, W. H., S. A. Teukolsky, W. T. Vetterling and B. P. Flannery. 1992. Numerical Recipes: The Art of Scientific Computing, 2nd ed., Cambridge Univ. Press, Cambridge, 963 pp.

Price, J. F. and M. Baringer. 1994. Outflows and deep water production by marginal seas, Prog. Oceanogr., *33,* 161–200.

Rhines, P. and W. R. Young. 1982. Homogenization of potential vorticity in planetary gyres. J. Fluid Mech., *122,* 347–367.

Robinson, A. R. and H. Stommel. 1959. The oceanic thermocline and the associated thermohaline circulation. Tellus, *11,* 295–308.

Salmon, R. 1986. A simplified linear ocean circulation theory. J. Mar. Res., *44,* 695–711.

—— 1990. The thermocline as an "internal boundary layer." J. Mar. Res., *48,* 437–469.
Salmon, R. and R. Hollerbach. 1991. Similarity solutions of the thermocline equations. J. Mar. Res., *49,* 249–280.
Samelson, R. and G. K. Vallis. 1997. A simple friction and diffusion scheme for planetary geostrophic basin models. J. Phys. Oceanogr., *27,* 186–194.
Schmitz, W. J., Jr. 1995. On the interbasin-scale thermohaline circulation. Rev. Geophysics, *33,* 151–173.
Stommel, H. and A. Arons. 1960. On the abyssal circulation of the world ocean-I. Stationary planetary flow patterns on a sphere. Deep-Sea Res., *6,* 140–154.
Stommel, H. and J. Webster. 1962. Some properties of the thermocline equations in a subtropical gyre. J. Mar. Res., *44,* 695–711.
Toggweiler, J. R. and B. Samuels. 1995. Effect of Drake Passage on the global thermohaline circulation. Deep-Sea Res., *42,* 477–500.
Toole, J., K. Polzin and R. Schmitt. 1994. Estimates of diapycnal mixing in the abyssal ocean. Science, *264,* 1120–1123.
Toole, J., R. Schmitt, K. Polzin and E. Kunze. 1997. Fine and microstructure evidence of boundary mixing above the flanks of a mid-latitude seamount. J. Geophys. Res., *102,* 947–959.
Tsuchiya, M., L. Talley and M. McCartney. 1992. An eastern Atlantic section from Iceland southward across the equator. Deep-Sea Res., *39,* 1885–1917.
Tziperman, E. 1986. On the role of interior mixing and air-sea fluxes in determining the stratification and circulation of the ocean. J. Phys. Oceanogr., *16,* 680–693.
Veronis, G., 1969. On theoretical models of the thermocline circulation. Deep-Sea Res., *16* (Suppl.), 301–323.
—— 1973. Model of the world ocean circulation: I, wind-driven, two-layer. J. Mar. Res., *31,* 228–288.
—— 1975. The role of models in tracer studies, Numerical Models of Ocean Circulation, Natl. Acad. Sci., Washington, D.C., 133–146.
Visbeck, M., J. Marshall and H. Jones. 1996. On the dynamics of isolated convective regions in the ocean. J. Phys. Oceanogr., *26,* 1721–1734.
Warren, B. 1990. Suppression of deep oxygen concentrations by Drake Passage. Deep-Sea Res., *37,* 1899–1907.
Welander, P. 1959. An advective model of the ocean thermocline. Tellus, *11,* 309–318.
—— 1971a. Some exact solutions to the equations describing an ideal-fluid thermocline. J. Mar. Res., *21,* 60–68.
—— 1971b. The thermocline problem. Phil. Trans. R. Soc. Lond. A., *270,* 415–421.
Winton, M. 1995. Why is the deep sinking narrow? J. Phys. Oceanogr., *25,* 997–1005.
—— 1996. The role of horizontal boundaries in parameter sensitivity and decadal-scale variability of course-resolution ocean general circulation models. J. Phys. Oceanogr., *26,* 289–304.
Winton, M. and E. Sarachik. 1993. Thermohaline oscillations induced by strong steady salinity forcing of ocean general circulation models. J. Phys. Oceanogr., *23,* 1389–1410.
Young, W. R. and G. Ierley. 1986. Eastern boundary conditions and weak solutions of the ideal thermocline equations. J. Phys. Oceanogr. *16,* 1884–1900.
Zhang, S., C. A. Lin and R. J. Greatbatch. 1992. A thermocline model for ocean-climate studies. J. Mar. Res., *50,* 99–124.

Received: *10 October, 1995;* revised: *15 October, 1996.*